Development of an Origami Inspired Composite Deployable Structure Utilizing Compliant Joints as Surrogate Folds

Samuel Porter Smith

A thesis submitted to the faculty of
Brigham Young University
in partial fulfillment of the requirements for the degree of

Master of Science

Spencer P. Magleby, Chair
Larry L. Howell
Andy George

Department of Mechanical Engineering

Brigham Young University

ABSTRACT

Development of an Origami Inspired Composite Deployable Structure Utilizing Compliant Joints as Surrogate Folds

Samuel Porter Smith
Department of Mechanical Engineering, BYU
Master of Science

This work presents the design and construction of a self-deployable, self-stiffening, and retractable (SDSR) space array from carbon fiber reinforced polymers (CFRP's) and a working prototype is demonstrated. The effort required developing principles for the design of high-strain composite flexural joints and their integration into angled composite panels. Designing LET arrays in angled panels is explored. Analysis of simple composite LET joints is presented for two degrees of freedom. Validation of the composite LET modeling is sought through numerical methods and empirical testing. Testing of several composite LET joint specimens is conducted and the results are reported. Results indicate that (while not as compact as their isotropic material counterparts) composite laminates can successfully use LET joints as surrogate folds.

Keywords: composites, deployable structures, origami, high-strain composites, LET Joints

ACKNOWLEDGMENTS

I express the greatest appreciation to my wife, Sierra, for supporting me through graduate school.

My graduate committee deserve trophies. I thank Dr. Magleby profusely for his patience and guidance in helping me through this process that I found so arduous. Also, Dr. Howell and Dr. George for their inspiring passion and dedication to subjects that have changed my life.

I'd also like to thank my peers, Nathan Pehrson, Pietro Bilancia, Lance Hyatt, Colton Inkley, Diana Bolanos, and Nathan Brown, without whom, I'd never have gotten this far.

This paper is based on work supported by the Air Force Office of Scientific Research grant FA9550-19-1-0290 through Florida International University

TABLE OF CONTENTS

LIST OF TABLES

LIST OF FIGURES

CHAPTER 1. INTRODUCTION

1.1 Motivation and Objective

In space missions, many methods and techniques are used to enable large deployable structures—such as solar arrays, antennas, and radiators—for power, communication, and heat regulation. With origami as inspiration, a new class of self-deployable, self-stiffening and retractable (SDSR) arrays have emerged in aerospace research. SDSR arrays do not require the aid of external support and actuation structures common in space applications, replacing them with compliant joints and reeling cables. The flexural joint used is an array of lamina emergent torsional (LET) joints, an innovative solution to attain large deflections needed for hinge-like motion in large foldable structures (a simple LET joint is shown in Figure 1.1).

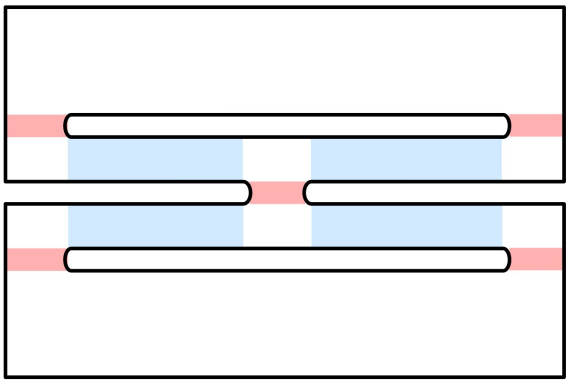

Figure 1.1: LET joint with torsional segments in blue and bending segments in red

An aluminum SDSR has been successfully modeled and demonstrated as shown in Figure 1.2. However, while aluminum is lightweight, SDSR technology can be greatly improved with more advanced, lighter weight materials. Carbon fiber reinforced polymers (CFRP) show promise for aerospace structures and this work attempts to understand the principles needed to successfully create SDSR's from composite materials. In general, the objective of this thesis is to develop

and demonstrate techniques for designing origami-based mechanical systems utilizing compliant composite joints with special application to deployable space structures.

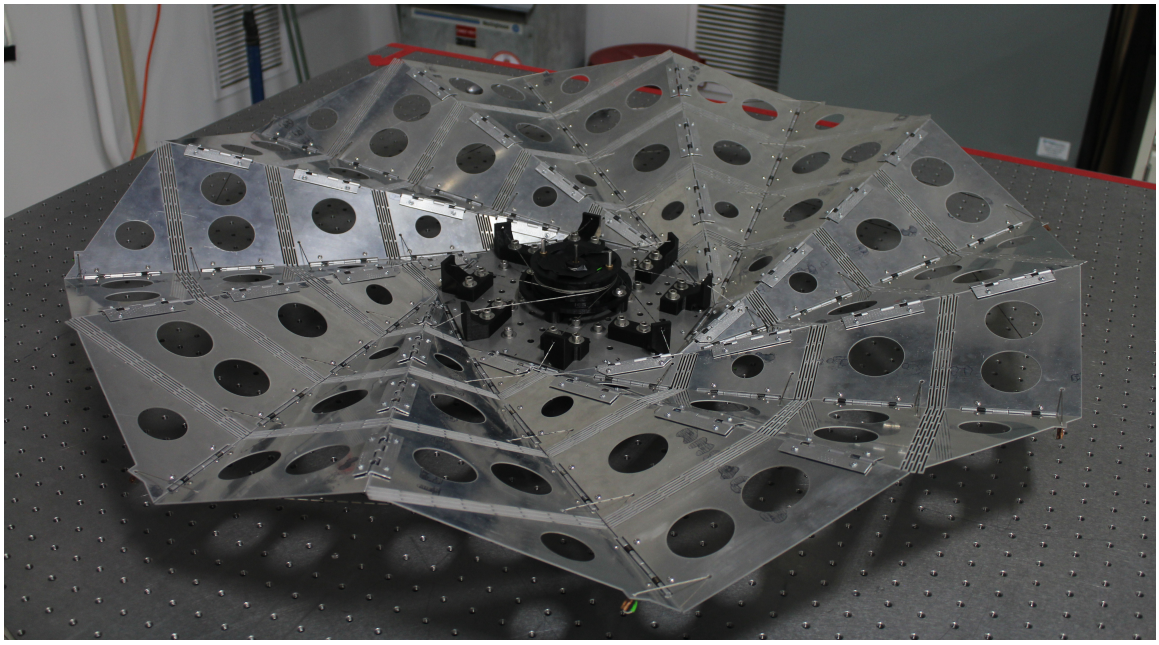

Figure 1.2: Aluminum SDSR

Two areas of interest arise while considering the adaptation of composite laminates for use in SDSR arrays. First, the LET joints used in an SDSR are integrated into angled sections. Only constant width arrays have been analyzed in literature. Second, composite LET's go against common practice since cutting into composites to create LET joints is not ideal for continuous fiber reinforced materials.

1.2 Thesis Outline

Chapter one considers LET arrays with irregular profiles for use in thick origami patterns such as the flasher pattern. This chapter also discusses LET arrays with irregular thickness. This chapter will be published in a conference such as IDETC.

Chapter two presents the adaptation of analytical models for use in composite laminates to LET joints. A MATLAB and ANSYS algorithm is used to numerically validate the use of

analytical solutions for LET joint characterization in two degrees of freedom. This chapter will be published in a journal such as Composites B.

Chapter three reviews previous work on SDSR's and presents the design and construction of a small scale composite SDSR. While only the array is explored here, the developed principles can be applied in other folding composite structures. This chapter is currently submitted for review at Scitech.

Chapter four concludes the thesis.

CHAPTER 2. ACCOMMODATING IRREGULAR PANEL PROFILES AND THICKNESSES IN LET JOINT ARRAYS

2.1 Introduction

Lamina emergent mechanisms (LEMs) are a class of compliant mechanism that are enabling innovative solutions to interesting engineering problems. The principal advantage of LEM's is they can be manufactured from flat materials, but their motion is out of the material plane [1]. LEM's are often utilized in MEMS [2] and origami inspired mechanisms [3] as surrogate folds. LEMs most often integrate lamina emergent torsional (LET) joints to achieve their kinematic motion. LET joints are simple compliant mechanisms that employ torsional beams in order to achieve folding or hinge-like motion in a compact area. One drawback to LET joints is that they have many degrees of freedom (see Figure 2.1) which causes excess motion (termed parasitic motion) other than the direction intended.

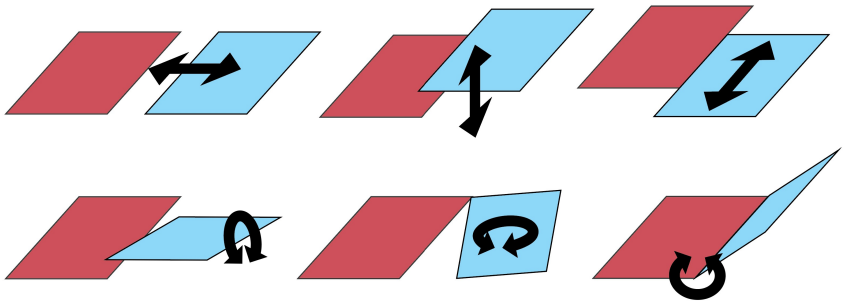

Figure 2.1: Representation of the six degrees of freedom for a LET joint

Generally, parasitic motion is undesirable, though, it could be considered an advantage if precise motion is not required or in an over-constrained system where some flexibility in the motion is needed to facilitate movement. To accommodate the folding of thick panels, large arrays of LET joints are usually needed [4] often exacerbating the parasitic properties of the joint. There are

methods to mitigate this motion such as membranes [5], hard stops [6], alternate beam geometries [7], and others.

LET arrays are easily used as surrogate folds when the regions being folded on each other have parallel sides, keeping the torsional segment geometry constant, i.e. a uniform LET array. This consistency inherently allows for homogeneous stresses/strains throughout the joint and, consequently, constant curvature along the joint can be achieved. A general analysis of uniform LET arrays was done by Pehrson [8]. Even though the LET arrays in the present work will not be uniform, the nomenclature used by Pehrson defining array sizes by the number of torsional segments in series and parallel is useful for this exploration.

As the literature on LET arrays expands, designers and engineers are finding more applications for them. A few ways in which products can benefit from using LET arrays as joints are to reduce part count, enhance manufacturability, enable more compact stowed states for shipping or storage, and facilitate a simplistic design with likeable aesthetics. Integrating LET arrays into products, however, can also lead to problems arising while adapting the compliant joints to irregularly shaped panels.

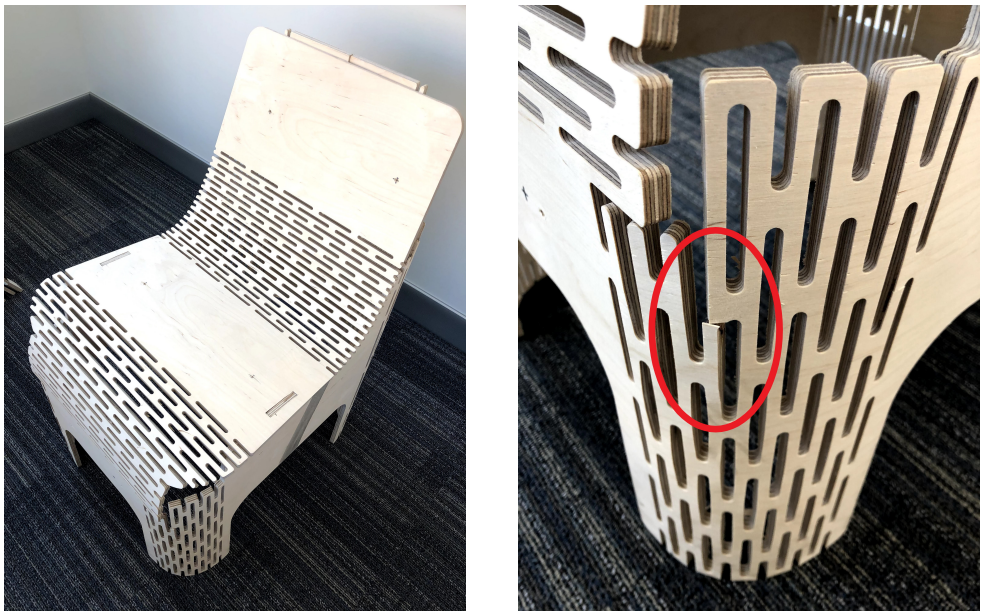

Figure 2.2: (Left) Plywood chair using LET arrays as hinges and (Right) broken torsional member in LET array

For example, in the design of a monolithic folding chair cut from plywood, failure of some of the torsional segments in the joints was observed as shown in Figure 2.2. In the transition from a narrower to a wider section of the array, the inconsistent torsional segment length caused stress in some segments more than others. This failure illustrates the non-intuitive way to use LET arrays as joints when the array and panel profile is angled, curved, or otherwise changes shape.

Another example where LET arrays can be used in irregular panels is a gore of an origami flasher (see Figure 2.3). LET arrays can be used on the triangular gores to create mountain or valley folds. If the torsional segment width and number of segments is held constant, the portion of the joint with longer torsional segments becomes less stiff. The variation in stiffness across the joint due to the change in length can foster premature failure. Naturally, it follows that by changing the other torsional segment dimensions (i.e. width and thickness), a constant stiffness LET array joint should be achievable.

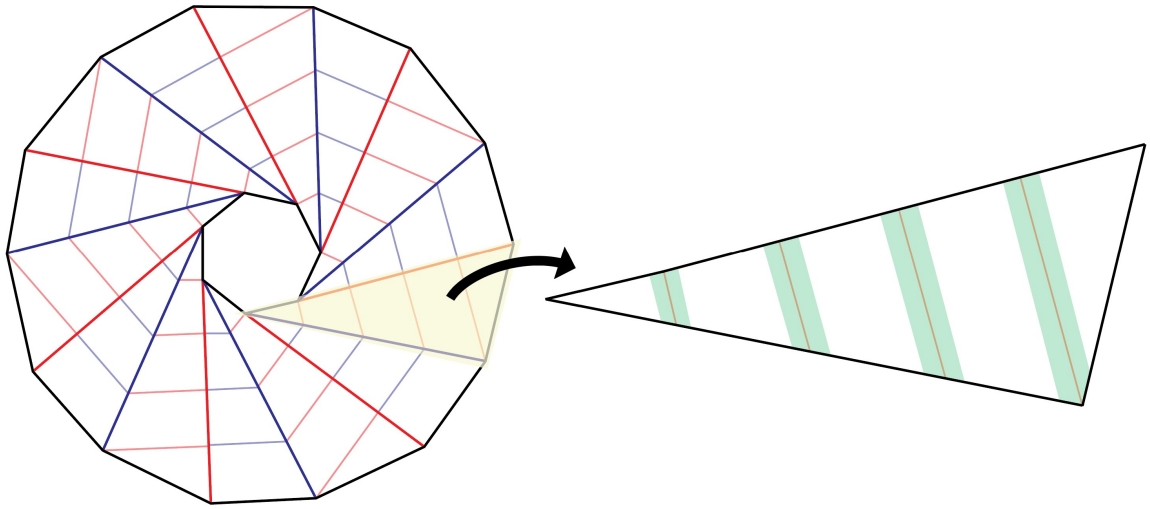

Figure 2.3: (Left) Origami flasher crease pattern with 7 major folds with (Right) LET array surrogate fold regions highlighted on an individual gore

While there are many interesting avenues in this realm yet to be analysed, this work focuses on the bending of LET arrays with irregular profiles. Only bending motion around the x-axis will be considered (Figure 2.4). Nelson shows that LET arrays can be used to achieve generalized cylindrical surface geometries [9]. This work builds upon those analytical principles.

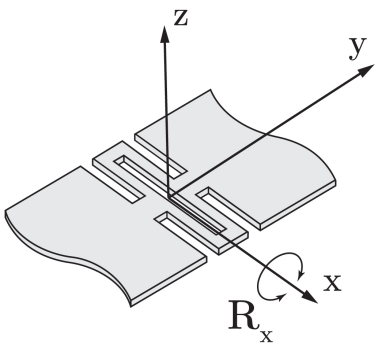

Figure 2.4: LET joint axes with bending about x-axis signified by reaction moment

2.2 Analysis

When LET arrays are bent or folded, the laminate takes on a curvature along the joint. Each set of torsional segments in parallel has an angular deflection θ, so the angular deflection of the entire LET array can be represented as a discreet set $\theta_{array} = \{\theta_1, \theta_2, \theta_3, ..., \theta_s\}$, where s is the number of torsional members in series.

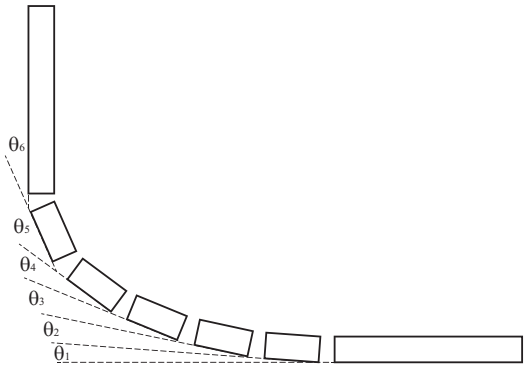

Figure 2.5: Each torsional segment corresponds to a deflection angle

The deflection of the LET array is the sum of the individual torsion beam angles. For a uniform array with uniform torsional segments, the angles are constant with the radius of curvature easily determined for a given load. For a non-uniform array—whether non-uniform in number of torsional elements (Figure 2.6) or in the dimensions of the torsional elements (Figure 2.7)—curvature may not be constant. For the purposes of the analysis in this work, each section

of torsional members in parallel (i.e. sections with the same length torsional members) will be considered independently.

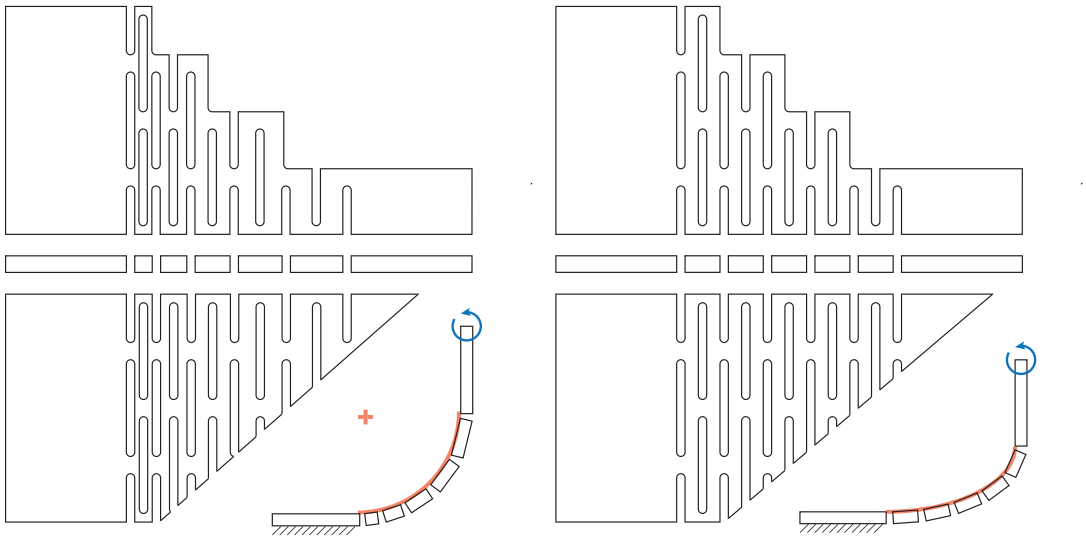

Figure 2.6: Curvature profiles corresponding with non-uniform number of torsional segments across LET array. Upper and lower LET arrays are analytically identical

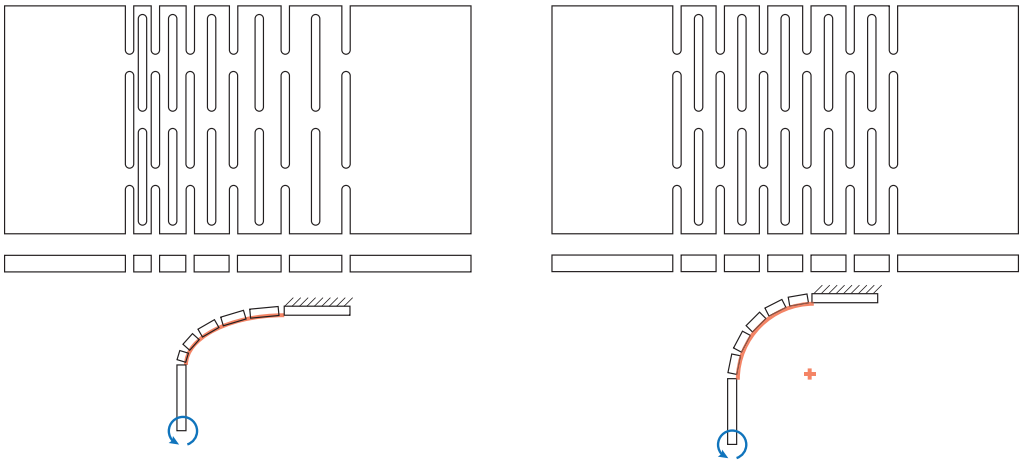

Figure 2.7: Curvature profiles corresponding with non-uniform torsional segment dimensions across angled LET array

Variation in stiffness across the joint causes non-uniform stresses throughout the array which in turn causes joint failure long before some torsional members have reached a critical point (as in Figure 2.2). Failure can be mitigated by changing the dimensions of the beams or number of beams in an array.

Each torsional member has a stiffness

$$K_T = \frac{wt^3\left(\frac{1}{3} - 0.21\frac{t}{w}\left(1 - \frac{t^4}{12w^4}\right)\right)G}{l_T} \tag{2.1}$$

as defined by Roark [10], or

$$K_T = \frac{fJ_TG}{l_T} \tag{2.2}$$

where

$$f = \frac{1.167z^5 + 29.49z^4 + 30.9z^3 + 100.9z^2 + 30.38z^{+}29.41}{z^5 + 25.91z^4 + 41.58z^3 + 90.43z^2 + 41.74z^{+}25.21} \tag{2.3}$$

with $z = w/t$ and

$$J_T = \frac{2t^3w_T^3}{7t^2 + 7w_T^2} \tag{2.4}$$

as defined by Chen [11].

2.2.1 LET Arrays in Angled Panels

When LET arrays are designed into triangular or angled quadrilateral panels (from here on referred to as angled panels), at least two choices exist for the designer. First, constant length torsional segments that vary in discreet integer amounts along the joint can be used as shown on the left of Figure 2.8. Secondly, variable-length torsional segments can be used as shown on the right.

The first solution is simpler both to conceptualize and to implement. An obvious drawback is the excess material not part of the array that sits on the edge of the joint, though this can be removed as shown in Figure 2.6. But this may or may not be admissible depending on the application.

To use the entire real estate for the LET array in an angled panel, care has to be taken as to where to define the bending and torsional segments. There may be other useful solutions, but

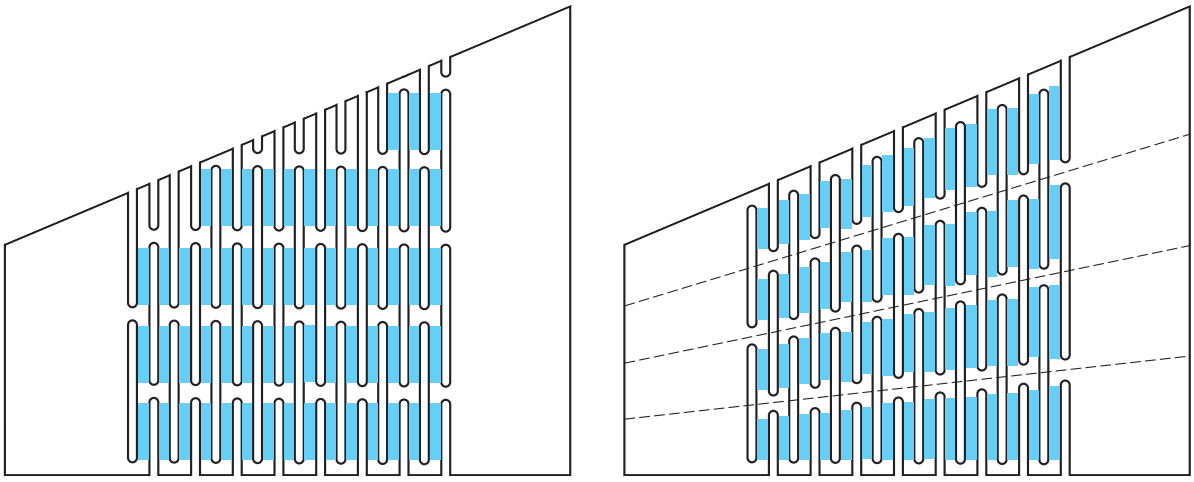

Figure 2.8: Constant (Left) and variable (Right) torsional beam length array in a diagonally cut panel illustrating the variation in torsional segments

placing the midpoint of the bending segments on equally spaced rays (Figure 2.8 Right) is a good starting point.

This equal ray spaced configuration has some quirks. The torsional segments don't increase linearly along the joint if the bending segments are kept perpendicular to the torsional segments. Figure 2.8 shows how the length increases linearly on the bottom row of torsional segments but staggers on the upper row. The steeper the angle, the more the staggering is noticeable. This variation could be mitigated with angled bending segments that follow the ray directions. Unfortunately, since bending segments are typically kept quite short and fillets are created by most manufacturing processes (which fillets also help with avoiding stress concentrations), this has a practical limit.

Regardless, the stiffness in each successive section of the LET array will be proportional to the number of parallel segments and the length and width of that section. Again, using Figure 2.8 as a reference, the left example has three distinct sections. Because the length is the same for each segment and only the number of segments in parallel changes, three separate widths would be used to make each segment have the same stiffness. Wider segments where there are fewer in parallel and narrower segments where there are more.

The example on the right of Figure 2.8 keeps the number of segments in parallel constant but varies the length. Each section is different so widths would vary for each section. The width for each section would increase as the segment length increases.

Table 2.1: Angled LET array torsional segment dimensions
for four different configurations

Variable Width Ray Aligned	
$L_{t,Avg}$	{1.11, 1.07, 1.03, 0.98, 0.94, 0.90, 0.86, 0.83, 0.79, 0.75, 0.72, 0.68, 0.65, 0.61}
W_t	{0.30, 0.29, 0.29, 0.28, 0.27, 0.26, 0.25, 0.24, 0.24, 0.23, 0.22, 0.22, 0.21 0.20}
Array Size	14s4p
Constant Width Ray Aligned	
$L_{t,Avg}$	{1.11, 1.07, 1.04, 1.00, 0.96, 0.92, 0.88, 0.85, 0.81, 0.77, 0.73, 0.69, 0.66, 0.62}
W_t	0.25
Array Size	14s4p
Variable Width Constant Length	
L_t	0.375
W_t	{0.21, 0.21, 0.21, 0.24, 0.24, 0.24, 0.24, 0.24, 0.24, 0.24, 0.30, 0.30, 0.30 0.30}
Array Size	3s5p+7s4p+4s3p
Constant Width Constant Length	
L_t	0.375
W_t	0.25
Array Size	3s5p+7s4p+4s3p

A mathematical tool was created to solve for the width values. A spreadsheet was used, though any software with a robust solver or optimization algorithm could be used. The stiffness of each section was calculated according to the dimensions of the array initially with constant thickness. The variation in stiffness in each section was then minimized using the solver's ability to adjust the width values.

Four 6 x 8 $in.$ angled LET arrays with a 22° slope cut in were designed for comparison purposes. Two arrays had constant length torsional segments with variable and constant width and two ray aligned arrays with variable and constant width torsion segments. Lengths and widths are shown in Table 2.1.

Similar to arrays of varying profile, the tool could also be used to find dimension values for arrays in materials of varying thickness. Figure 2.9 shows qualitatively how the width of the torsional member should vary with thickness across the LET array to achieve uniform stiffness throughout. A panel with varying thickness and profile is an obvious extension of the two previously discussed principles. Depending on which direction the thickness and profile increases,

the width accommodations could either be diminished or magnified. As each of the sections are considered, a geometry can be found to allow for a joint with uniform stiffness.

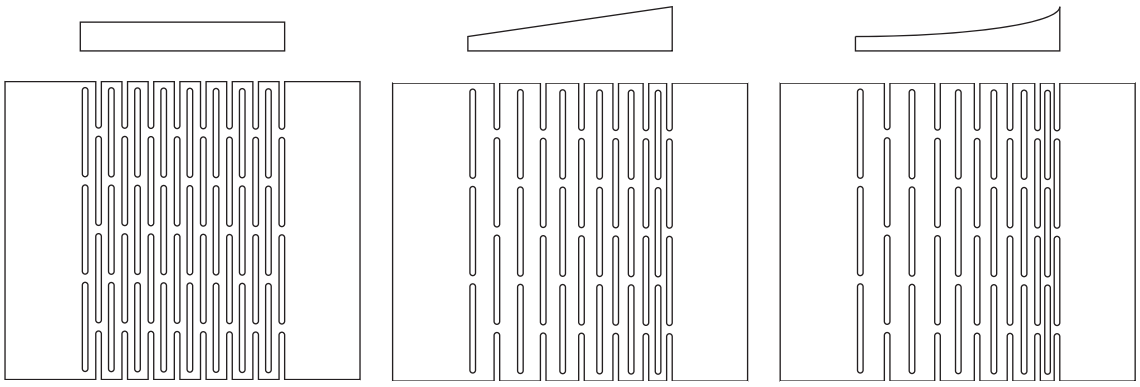

Figure 2.9: Notional representation of LET arrays, each with constant curvature having (Left) constant, (Middle) linearly increasing, and (Right) non-linearly increasing thickness

2.2.2 Numerical Analysis

Four angled LET arrays were modeled in CAD and meshed with standard auto-generated solid elements. The shorter end was fixed starting 0.25 inches from the first set of bending segments. A moment of 2 Nm was applied to the long end. The moment imparted a total angular deflection of 85°. The results from the numerical simulations are shown in Table 2.2. Using the ray aligned method creates much more uniform torsional segment stiffness as shown by the angular displacement variance. The maximum stress in the ray aligned variable width angled array is reduced 22.3% from the standard constant length constant width angled array configuration. However, just using the ray aligned configuration with constant width segments is a significant improvement.

2.3 Prototyping

The four LET arrays were milled from Polypropylene for demonstration. Polypropylene is a good material choice for compliant mechanisms. This is thought to be caused by its isotactic small methyl pendant group, which facilitates quick and easy re-crystallization of the chemical

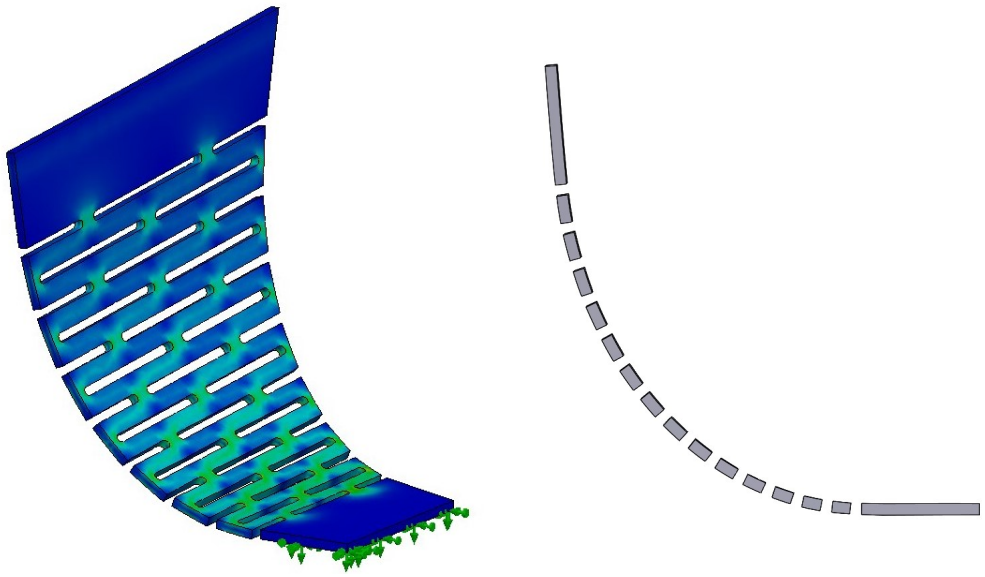

Figure 2.10: Simulation of ray aligned variable-width angled LET array with cross section view showing curvature

Table 2.2: Comparison of FEA results of the four angled LET array configurations

	Var. Width Ray Aligned	Const. Width Ray Aligned	Var. Width Const. Length	Const. Width Const. Length
θ_{avg} (Deg)	5.67	5.66	5.67	5.65
Angle Variance (Deg)	1.76	1.73	2.16	3.22
θ_{min} (Deg)	3.26	3.77	3.68	3.10
θ_{max} (Deg)	7.07	7.30	8.66	9.28
Range (Deg)	3.81	3.53	4.98	6.18
θ_{Total} (Deg)	85.12	84.92	85.01	84.82
$Stress_{max}$ (MPa)	21.30	23.11	28.58	27.42

microstructure after elastic deformation. Other plastics either blush or craze under bending strain or are less elastic and thus more prone to brittle failure [12]. Crazing is easily noticeable when 3D printing compliant mechanisms using materials like PLA, though it is still a valuable material for prototyping compliant mechanisms.

As seen in Figures 2.11 and 2.12, the bent specimens appear fairly constant and correlate well with the FEA. While the prototypes in this work only demonstrate isotropic plastic, it follows that similar methods (if not the same ones) can be used for anisotropic materials such as plywood

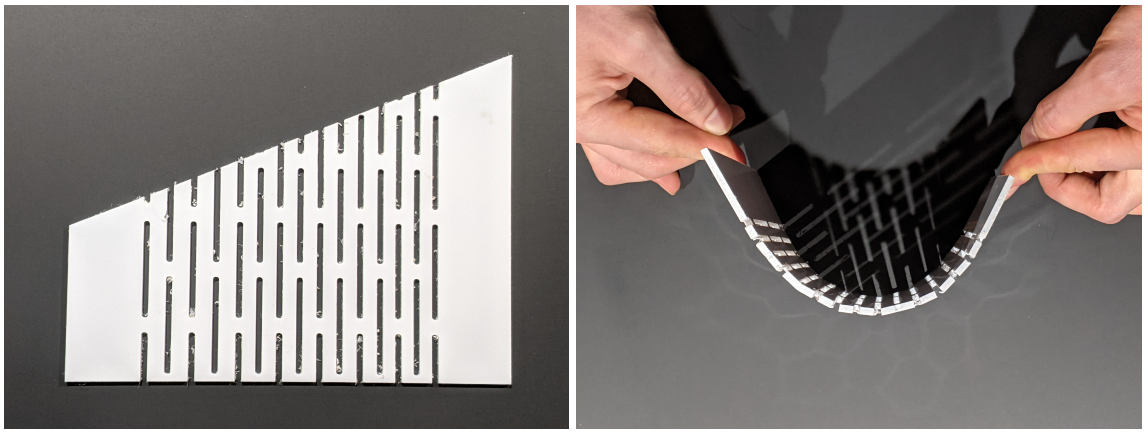

Figure 2.11: (Left) Angled LET array with constant length and variable-width torsional segments and (Right) same array with nearly constant curvature when bent

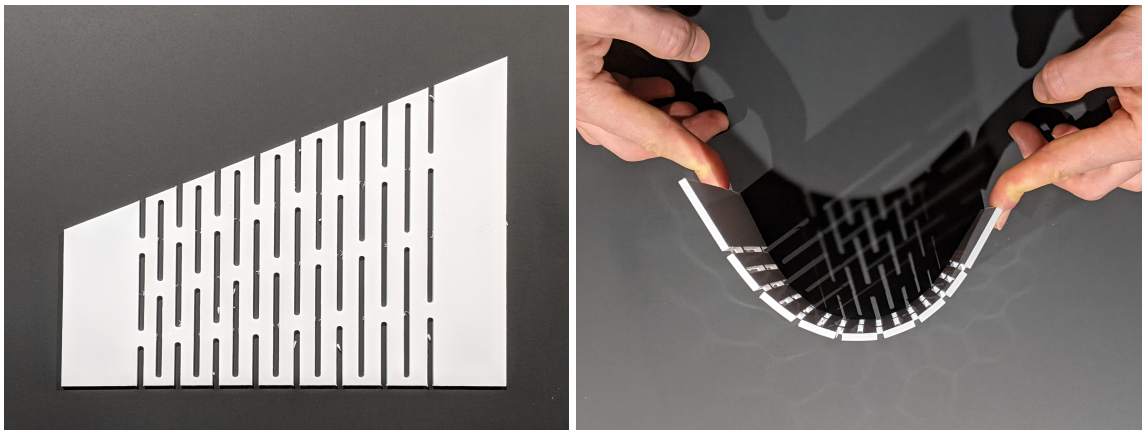

Figure 2.12: (Left) Angled LET array with variable-length and Variable-width torsional segments and (Right) same array with nearly constant curvature when bent

or composite laminates. Further analysis and testing would need to be done to fully characterize those kinds of materials.

2.4 Conclusion

This work is successful in describing a method to adapt LET arrays into non-uniform panel shapes. This helps the designer incorporate LET arrays as folding joints into more complex structures and mechanisms than previously possible, especially those created from irregular shaped sheets.

CHAPTER 3. ACCOMMODATING CARBON FIBER REINFORCED POLYMER LAMINATES IN LET JOINTS

3.1 Introduction

Compliant mechanisms take advantage of the elastic nature of materials that allow for motions without permanent deformation. Compared to traditional rigid-body mechanisms, they are often easier to manufacture, have fewer parts, require less maintenance, and can be very strong despite their flexibility [13]. Compliant mechanisms are becoming more common in everything from consumer goods, such as plastic flip-top bottle caps and buckles, to niche high-end applications, such as monolithic 3D printed titanium hinges [14] or inflatable enclosures on spacecraft [15].

Many metals and plastics are well suited for compliant mechanisms because they maintain a high strength to flexibility ratio (e.g., polypropylene, titanium, etc.). It follows that the methods for characterizing compliant mechanisms generally assume isotropic materials, however, anisotropic materials could also be used given the proper analysis.

Recent research has shown the effectiveness of using thin fiber reinforced composite shells that can undergo high-strains without failure [16]. Stiff structures can be achieved through the cross-sectional geometry (i.e. a large area moment of inertia) while the thin shell allows for collapsibility. Split tube and tape spring hinges [17], coilable booms [18], and other structures have been developed.

In design of origami-inspired engineered products, thin composite hinges could be attached to rigid panels to achieve folding motion [19]. However, using principles of compliant mechanisms, a hinge and folding panels could be made from a single sheet of material. Composite laminates are readily available in the commercial market and are easy to machine. In general, composites are machined as little as possible as machining destroys the continuous fibers and the superior material properties that come with them. The question arises, how can composite sheets be modified to obtain hinge-like motion?

The objective of this work is to explore flexural composite geometries for use in composite panels. This will be accomplished by adapting methods for designing LET joints in isotropic materials [20] for use in anisotropic materials such as fiber reinforced composite laminates. LET joints can move in 6 degrees of freedom, translation and rotation about each axis. Because only one or two DOF's are desired, the other DOF's are considered parasitic. This work will focus on only two degrees of freedom, namely, rotation about the *y* and *x* axes as shown in Figure 3.1.

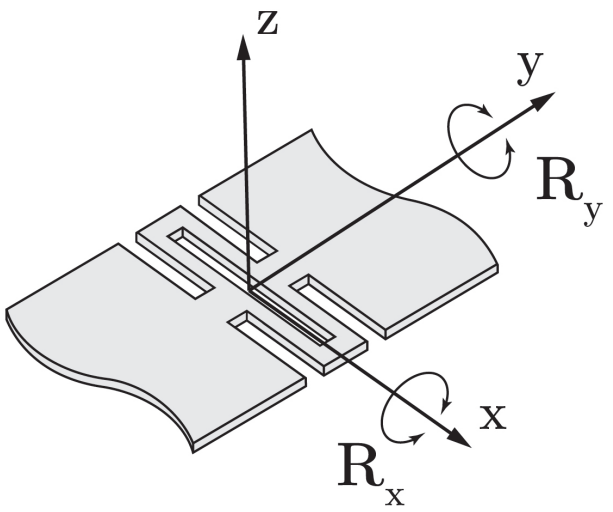

Figure 3.1: Orientation of axes on LET joint and motions of interest

3.2 Background

3.2.1 Strained Joints

In origami inspired engineering, methods have been developed to accommodate thick materials in folding patterns that retain the characteristics of zero-thickness folding models [21]. Furthermore, many joint designs that accommodate the thickness of common engineering materials in folding include regionally sandwiched strained joints [22], tapered panels [23], hinge shifts [24], offset panels [25], SORCE Joints [26], membranes [27], and 4-bar linkages [28]. Flexure joints are often used in origami inspired applications as surrogate folds [20].

3.2.2 LET Joints

A common LEM component is the lamina emergent torsional (LET) joint. LET joints are used particularly when trying to induce folding motion in sheet materials to emulate two panels connected with a hinge. This can be accomplished easily using subtractive manufacturing methods to create the LET joint and hinges.

A LET joint can be thought of as a network of simple beams, each with an equivalent bending or torsional spring stiffness. An equivalent stiffness of the entire joint can be determined by considering the individual beams as springs in parallel or in series according to each beam's respective position in the joint [29].

3.2.3 Fiber Reinforced Composite Laminates

Carbon fiber is synonymous with high-performance, high-cost applications. When epoxies or other polymers are reinforced with carbon fibers, they are stiff, strong, lightweight and have remarkably tailor-able properties for different applications. Unfortunately, this versatility comes with a cost and it can be difficult and time consuming to design robust and efficient composite parts.

In industry, quasi-isotropic laminates are often used to make engineering calculations simpler. Using quasi-isotropic CFRPs has led to the nickname "black aluminum" because many of the unique properties of CFRPs are often ignored for ease of calculations. Graduate students are not much different from industry in regard to desiring analytical simplifications. Laminate analysis simplifications, though not always ideal, are very often desirable. Symmetric laminates reduce extension-shear coupling—strains caused by bending moments and/or curvatures caused by in-plane loads. Balanced laminates reduce shear-extension coupling. Symmetric and balanced laminates are much easier to analyse and make for better composite sheets.

3.3 Joint Folding Stiffness Characterization

3.3.1 Design of Composite Laminates for LET Joints

Composite laminate design can be an arduous task. Many design guidelines and rules-of-thumb have been developed to help engineers make better decisions when designing new components like rule of mixtures, Hart-Smith, and Classical Laminate Analysis [30]. For the sake of analytical simplicity, a ply schedule of $[0°/90°, +45°/-45°]_s$ was used for the LET joints in this study. Purely unidirectional laminates would be even simpler for analysis but are impractical for actual composite parts due to the severe anisotropy.

Effects of high aspect ratio torsion members

A trade-off exists when trying to paramaterize a torsional beam in a composite laminate. Torsional stiffness models generally become less accurate as a cross section looks less like a circle– e.g. a long thin rectangle. However, thin composite beams with higher aspect ratios (long thin rectangles) are less susceptible to delamination. Because the trade off between accurate modeling and robustness against laminate failure will obviously tend toward more robust parts, empirical data will be critical to verify the torsional models and understand their limitations.

Torsion of Composite Beams With Rectangular Cross Section

To analyze the composite flexure joint, analysis of the component beams must agree to a certain extent with the assumptions made for isotropic joints; namely, that the elastic force-displacement behavior of the material in torsion is linear. For small deflections in the bending segments, this is an accurate assumption. For large deflections in the torsional beams, the model introduced by Lekhnitskii [31] is the linear relationship $k_t = G_{xy}\frac{ab^3}{L}\beta$ where

$$\beta = \frac{32a^2G_{yz}}{\pi^4 b^2 G_{xy}} \sum_{n=1,3,5,\ldots}^{\infty} \frac{1}{n^4}\left[1 - \frac{2a}{n\pi b}\sqrt{\frac{G_{yz}}{G_{xy}}}tanh\left(\frac{n\pi b}{2a}\sqrt{\frac{G_{xy}}{G_{yz}}}\right)\right] \tag{3.1}$$

Because the accuracy of this torsional model is potentially limited in its range (which is is not given in the literature), initial confidence in using it for large deflections was low. Physical

testing of composite strips in torsion was used to better understand the range where the linear assumption holds true.

Two different laminates strips were tested using a torque gauge and encoder with one end attached to a linear bearing as shown in Figure 3.2. The strip layup and dimension were $[(90/0)_2/\overline{90}]_s$ and $[(0/90)_2/\overline{0}]_s$, with dimensions, $83 \times 10.5 \times 0.65\,mm$. Torque data through angular displacement was recorded using LabView.

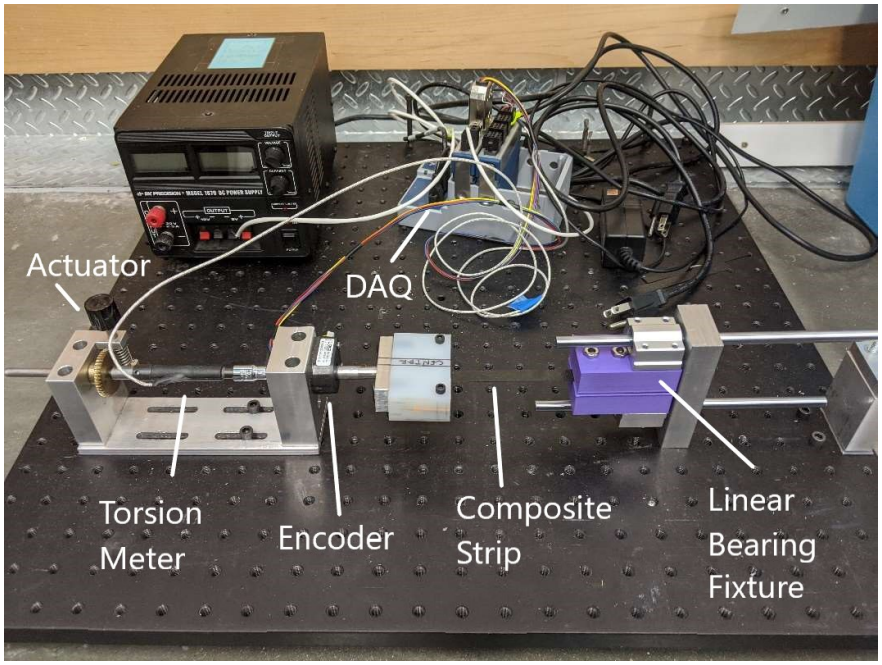

Figure 3.2: Twisting test configuration

3.3.2 Composite Strip Test Setup

Testing was also done with one end of the composite strip rigidly fixed to verify boundary condition assumptions. Even though the boundary conditions are different, the results are exactly the same. The results shown in Fig 3.3 illustrate a model constraint when designing LET joints. Note the elastic region of composite strips in torsion is linear for relatively large displacements. Since the linear assumption holds for deflections $(\theta <= 45^\circ)$, the LET joints in this paper will be limited to torsional beams in that range.

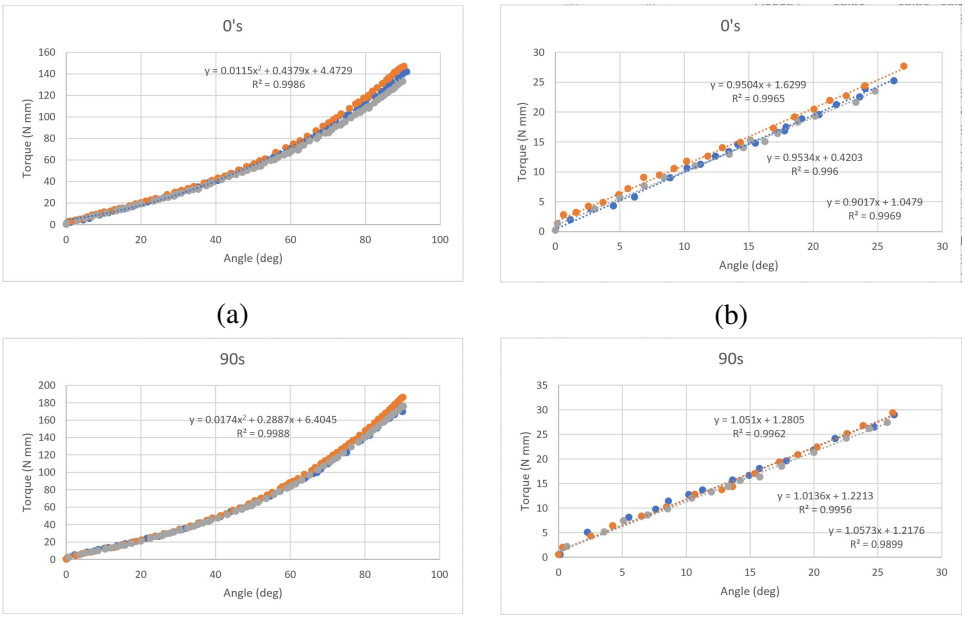

Figure 3.3: Torsion-angular displacement chart of single composite strip

3.4 LET Joint Testing

LET Joints were fabricated from a CFRP laminate (Hexcel IM7 plainweave fiber with epoxy matrix) for physical testing. Three specimens of each size were tested in torsion around both the x and y axes. The dimensions of the specimens tested ranged in torsional segment width from 1 to 6 $1/16$ of an inch—measurements are kept as multiples of $1/16$ inch to aid in data organization. The torsional segment length was constant at 0.75 inches. The bending segments were 0.125 inches long and 0.25 inches wide. The thickness of each specimen was $1/16$ inch.

The test setup was very similar to the laminate strip as shown in Figure 3.4. The data acquisition software and input mechanism were the same and only fixtures to accommodate the LET joint geometry were needed. The folding test also incorporated an extension arm to serve as a moment simulation, though only the twisting setup is shown.

3.4.1 Torsion About X-Axis (Folding)

The resulting stiffnesses are presented in Figure 3.8 with Lekhnitski's model as well as the Finite Element Analysis (FEA) model. Each plot represents three specimens each loaded to 30

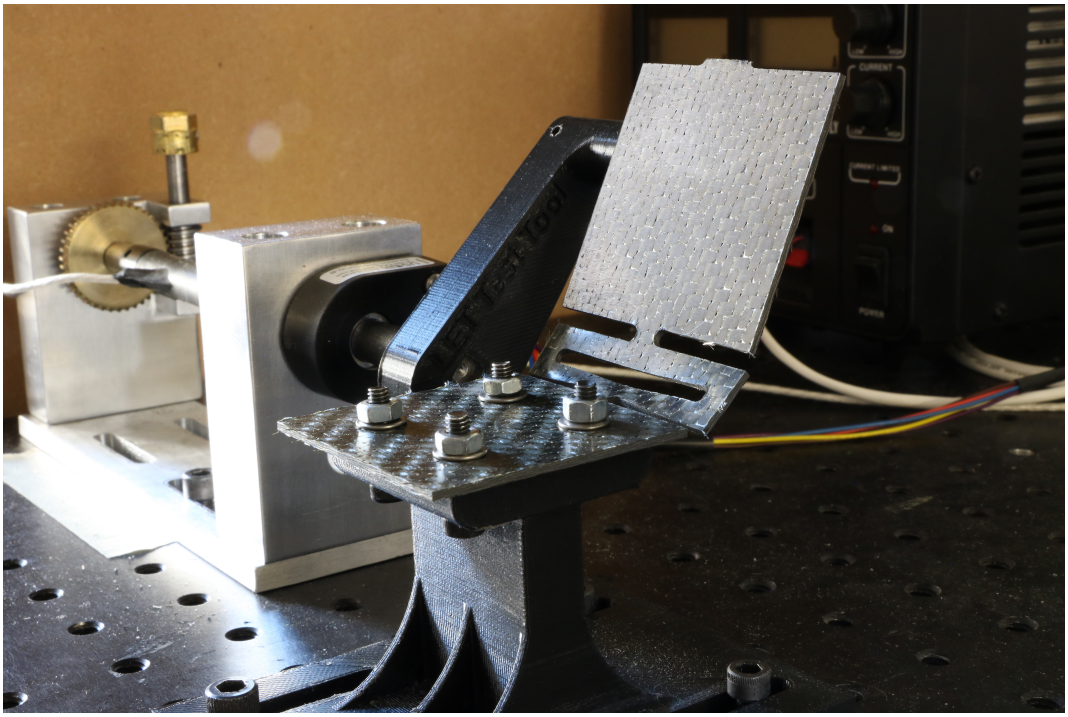

Figure 3.4: Folding test configuration

degrees three times. The plots show linear stiffness equivalents that are similar to the analytical model. There is some hysteresis when unloading each specimen, but subsequent loadings are not affected.

Material properties were estimated using the 6/16" specimen results. First, G_{xy} and G_{yz} were estimated using Lekhnitski's model, where G_{xy} = 1.5 GPa and G_{yz} = 1.3 GPa. Those values were used for each of the different sized specimens with good results. The estimated G_{xy} and G_{yz} were then used in the numerical model where the orthotropic moduli were also estimated using the 6/16" joint data. The values found were E_x = 2400 MPa, E_y = 2400 Mpa, and E_z = 500 MPa. The modulus values are low in general for the type of composite used, but the expired prepreg used for the laminate is likely the culprit there. Regardless, the estimated values were sufficient and the numerical model correlated well with the analytical model as well as testing of the different sized specimens.

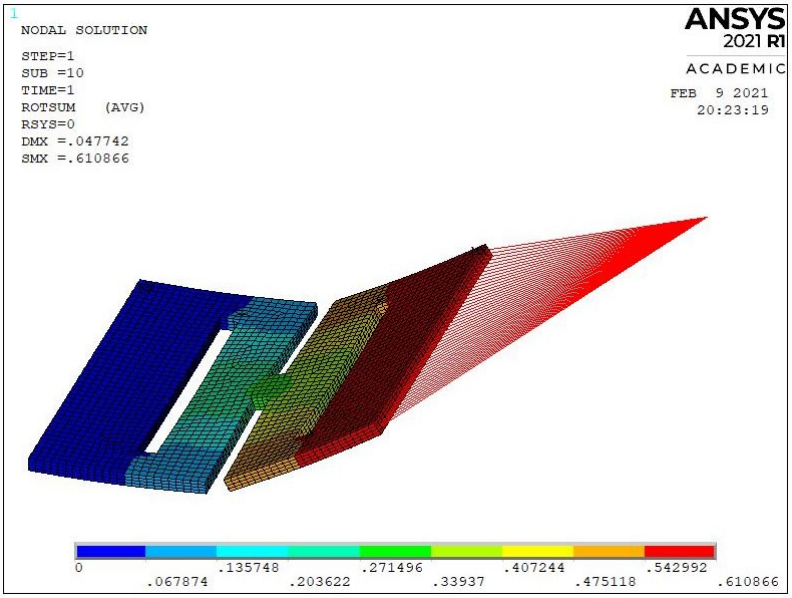

Figure 3.5: LET joint meshed with shell elements and displaced 35 degrees about x-axis

3.4.2 Torsion About Y-Axis (Twisting)

The twisting test setup is shown in Figure 3.6. The resulting stiffness in torsion about the y-axis are presented in Figure 3.9. The stiffness of the LET joints in this degree of freedom is analysed differently than the folding state. The torsional segments are now bending segments with fixed end boundary conditions and the bending segments are now the torsional segments. Because of the geometry used, the tests were limited to 15 degrees. The larger data variation in the first sample shown are from unintentionally delaminating the specimen at the single bending segment in the middle of the joint—a weakness of the joint configuration selected for testing.

3.4.3 Numerical Analysis

ANSYS Mechanical APDL was used for the FEA. The LET geometry was meshed with 181 shell elements representing the four layer orthotropic laminate [0, 45]s using the material properties mentioned before (macro in the appendix). A node for the angular displacement load was attached using rigid elements to one edge of the joint. The displacement load was applied and the reaction moment at the point was output for 5, 15, 25, and 30 degrees.

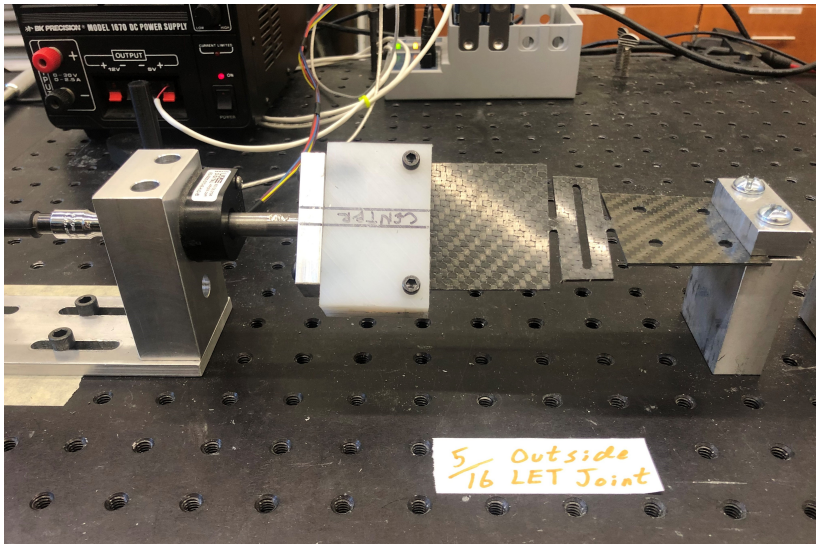

Figure 3.6: Twisting test configuration

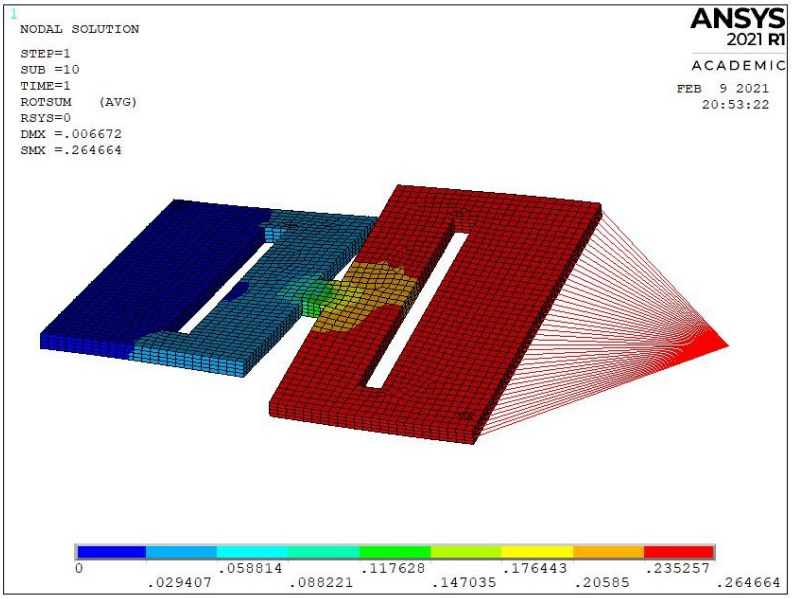

Figure 3.7: LET joint meshed with shell elements and displaced 15 degrees about y-axis

Stiffness measurements were output for each FEA iteration and are reported in Tables 3.1-3.4. The stiffness values in folding are consistent within a maximum of 0.05 N/deg, or 0.3% variation. The stiffness values in twisting are repeatable within a maximum of 0.93 N/deg, or 2.6% error, however most values are within 1% variation.

Table 3.1: FEA stiffness outputs for folded inside LET in newtons/degrees

Width\Angle	5	15	25	35
1/16	2.54	2.53	2.54	2.53
2/16	8.34	8.33	8.34	8.34
3/16	13.58	13.59	13.60	13.61
4/16	17.70	17.71	17.72	17.73
5/16	20.64	20.65	20.66	20.69
6/16	22.80	22.82	22.84	22.86

Table 3.2: FEA stiffness outputs for folded outside LET in newtons/degrees

Width\Angle	5	15	25	35
1/16	2.48	2.47	2.47	2.47
2/16	8.04	8.05	8.05	8.05
3/16	12.52	12.52	12.52	12.53
4/16	15.90	15.90	15.91	15.92
5/16	17.90	17.91	17.92	17.93
6/16	19.94	19.95	19.96	19.98

Table 3.3: FEA stiffness output for twisted inside LET in newtons/degrees

Width\Angle	4	8	12	16
1/16	35.93	36.11	36.43	36.86
2/16	46.40	46.50	46.65	46.86
3/16	51.93	52.00	52.12	52.29
4/16	51.03	51.10	51.21	51.36
5/16	49.73	49.79	49.89	50.04
6/16	46.20	46.26	46.37	46.52

Table 3.4: FEA stiffness output for twisted outside LET joint in newtons/degrees

Width\Angle	4	8	12	16
1/16	21.55	21.56	21.58	21.61
2/16	27.40	27.41	27.44	27.47
3/16	30.08	30.09	30.11	30.15
4/16	29.58	29.60	29.63	29.69
5/16	28.28	28.31	28.35	28.40
6/16	26.25	26.29	26.33	26.38

3.5 Design Considerations

A few qualitative lessons learned while creating composite LET joints.

LET joint geometries should favor minimizing the number of torsional segments. Torsional segments that are long and thin, with relatively large widths are the most robust against delamination. Unfortunately, this can increase parasitic motion in some designs (e.g. a single torsion member) or easily create larger than desired joint dimensions. Dropping plies about the joint region to reduce thickness can decrease the bend radius. Such ply drops are best buried within continuous plies and spread as far apart as possible to minimize delamination-inducing stress concentrations. Multi-material composites can be promising, for example, replacing external plies with glass reinforcements can reduce joint stiffness while still maintaining high strength properties.

Overall, the application will determine whether or not a composite is suitable. LET joints in isotropic metals and plastics can outperform composites when trying to create monolithic joints in a stiff panel with uniform thickness when a compact joint is required. Although compact dimensions and tight bend radii may not be the greatest advantage of composite LET joints, the other advantages of composites over isotropic materials remain. Corrosion resistance, thermal stability, RF compatibility, stiffness, weight, strength, and the general design freedom of tailorable orthotropic laminate materials.

3.6 Conclusion

The analysis and testing results of this small subset of CFRP LET joints enhance confidence in using FRP's in origami inspired mechanisms and structures. Because composites properties are extremely tailorable, the advantages of using composites can be leveraged against any inherent material shortcomings.

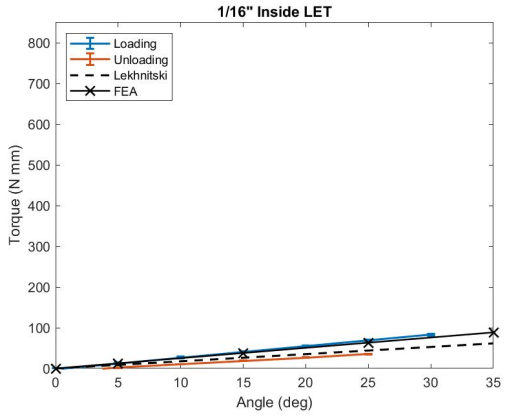
1/16" Inside LET
Loading
Unloading
Lekhnitski
FEA
Torque (N mm)
Angle (deg)

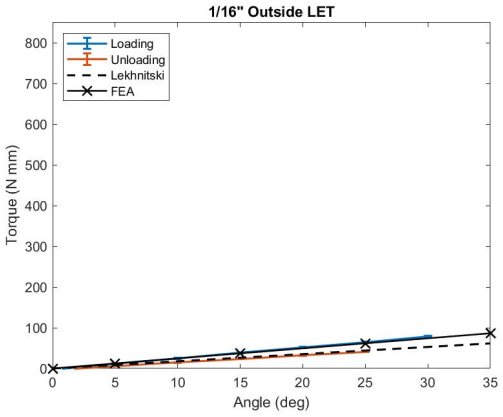
1/16" Outside LET
Loading
Unloading
Lekhnitski
FEA
Torque (N mm)
Angle (deg)

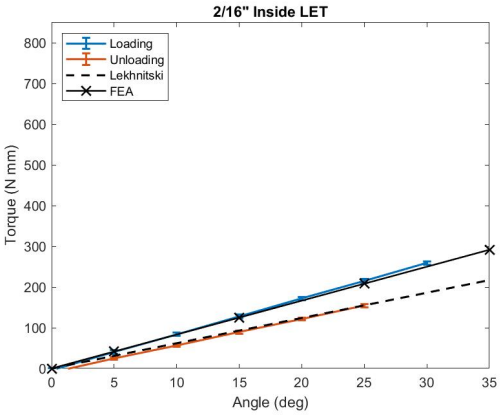
2/16" Inside LET
Loading
Unloading
Lekhnitski
FEA
Torque (N mm)
Angle (deg)

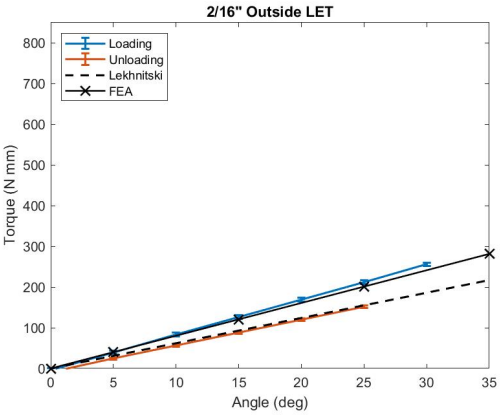
2/16" Outside LET
Loading
Unloading
Lekhnitski
FEA
Torque (N mm)
Angle (deg)

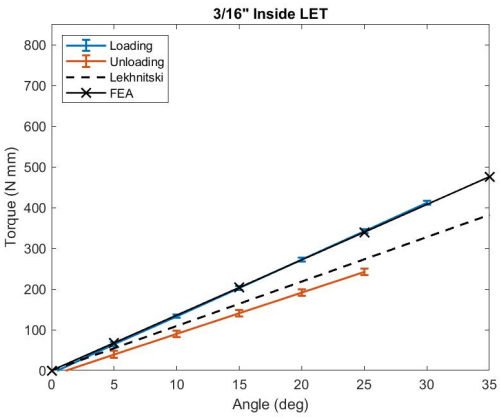
3/16" Inside LET
Loading
Unloading
Lekhnitski
FEA
Torque (N mm)
Angle (deg)

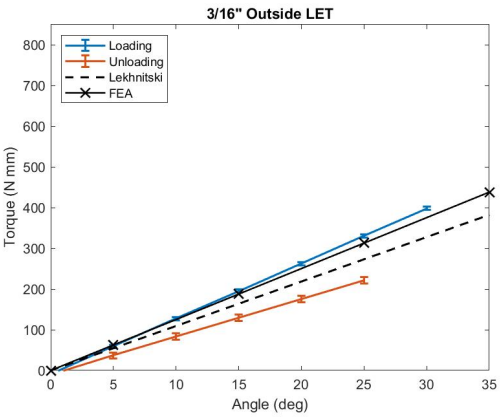
3/16" Outside LET
Loading
Unloading
Lekhnitski
FEA
Torque (N mm)
Angle (deg)

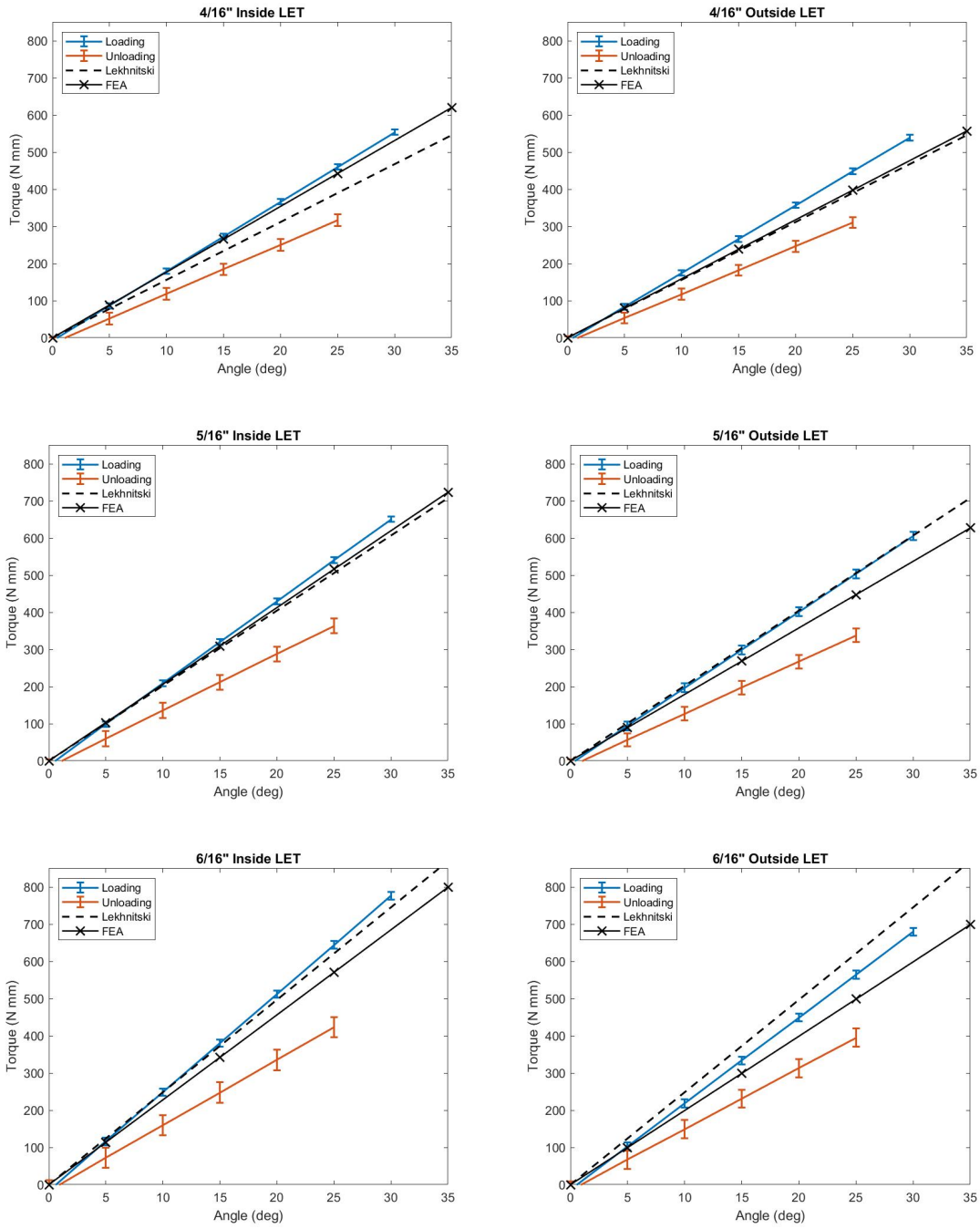

Figure 3.8: LET joint x-axis torsion-displacement plots

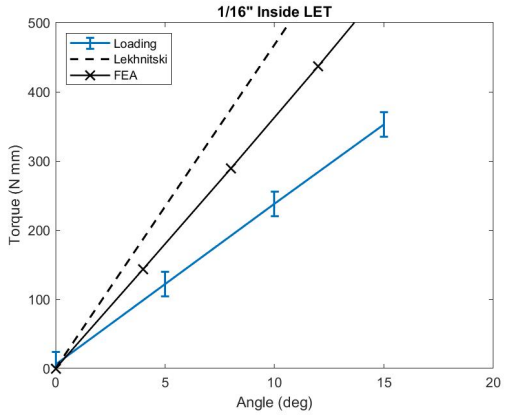
1/16" Inside LET
Loading
Lekhnitski
FEA
Torque (N mm)
Angle (deg)
0
100
200
300
400
500
0
5
10
15
20

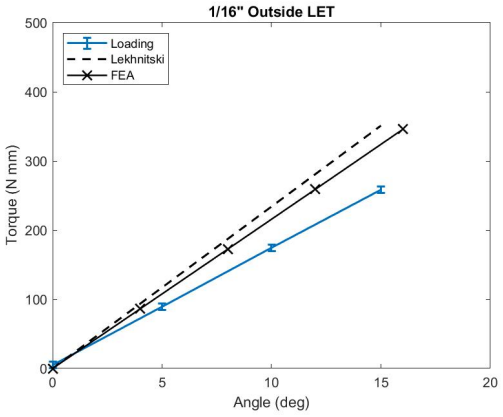
1/16" Outside LET
Loading
Lekhnitski
FEA
Torque (N mm)
Angle (deg)
0
100
200
300
400
500
0
5
10
15
20

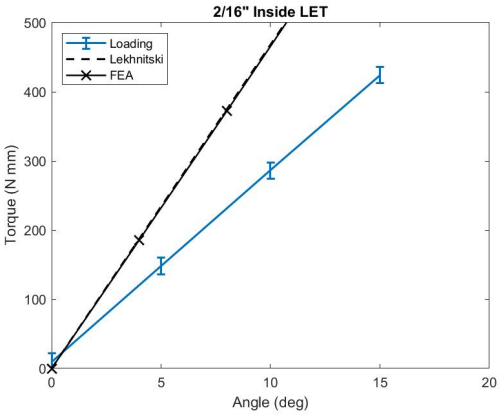
2/16" Inside LET
Loading
Lekhnitski
FEA
Torque (N mm)
Angle (deg)
0
100
200
300
400
500
0
5
10
15
20

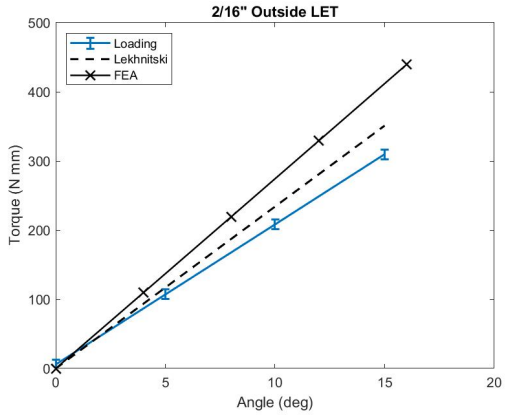
2/16" Outside LET
Loading
Lekhnitski
FEA
Torque (N mm)
Angle (deg)
0
100
200
300
400
500
0
5
10
15
20

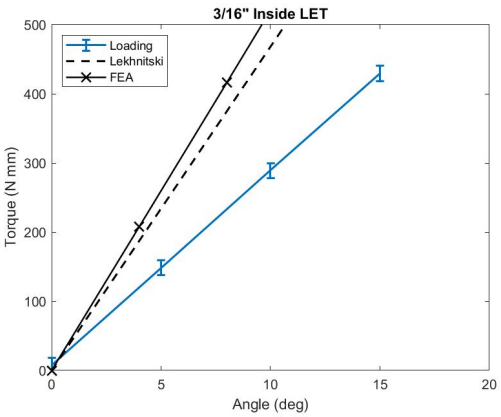
3/16" Inside LET
Loading
Lekhnitski
FEA
Torque (N mm)
Angle (deg)
0
100
200
300
400
500
0
5
10
15
20

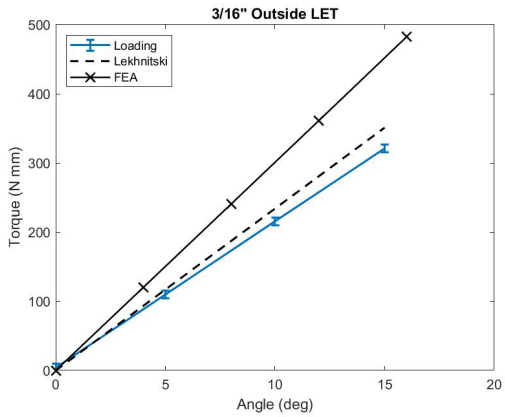
3/16" Outside LET
Loading
Lekhnitski
FEA
Torque (N mm)
Angle (deg)
0
100
200
300
400
500
0
5
10
15
20

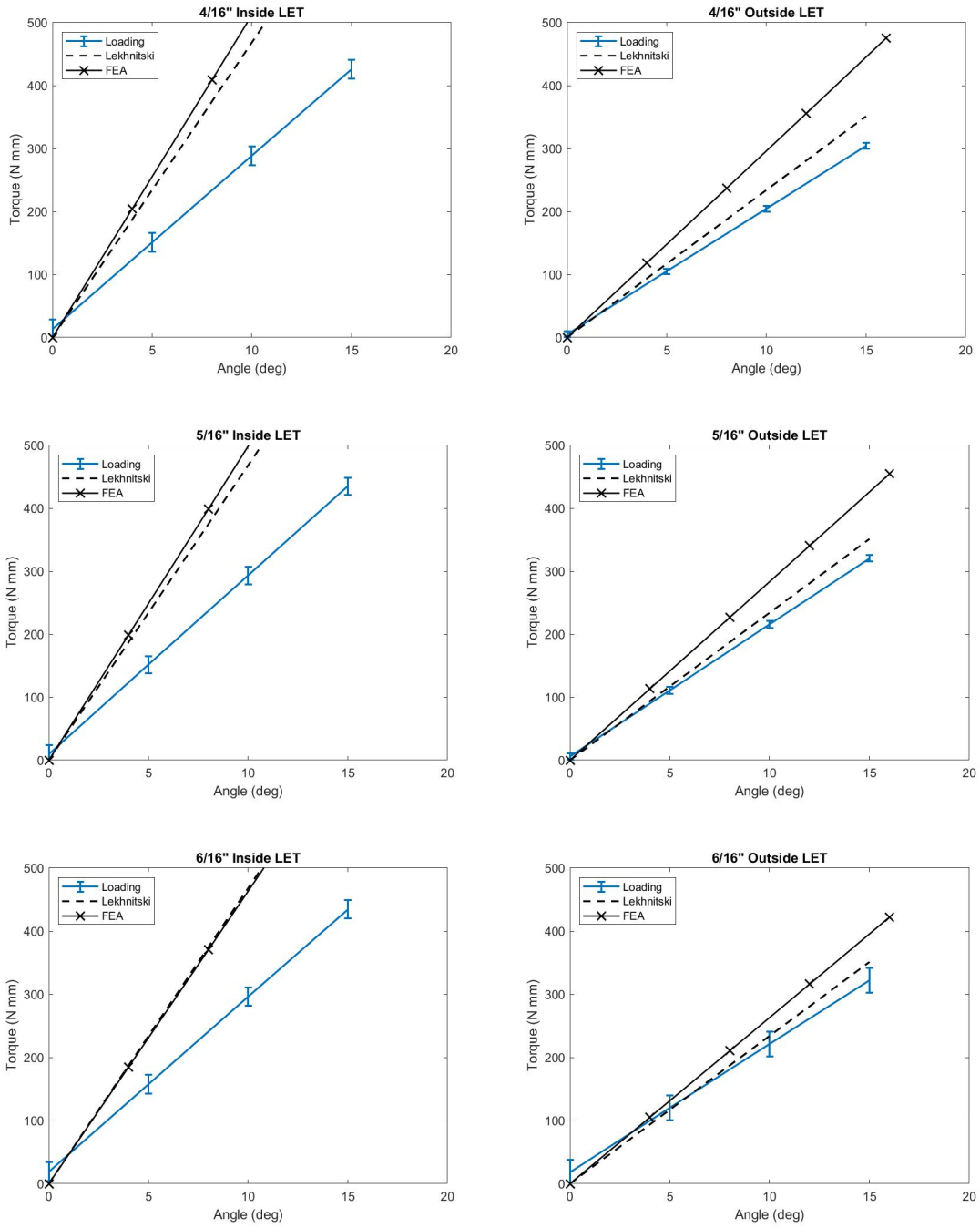

Figure 3.9: LET joint y-axis torsion-displacement plots

CHAPTER 4. PRINCIPLES FOR DESIGNING AN ORIGAMI-INSPIRED DEPLOYABLE COMPOSITE SPACE STRUCTURE WITH HIGH-STRAIN COMPOSITE LAMINATE JOINTS

4.1 Introduction

Some space missions rely on the ability to fold up large sheet-like structures, such as solar arrays, on earth and deploy them once in space. Maintaining stiffness at full deployment is a major obstacle in these large arrays. Typically, these arrays are actuated and stiffened through mechanisms such as trusses [32, 33] and booms [34–39]. Unfortunately, support and actuation structures occupy valuable volume that could otherwise be used for more useful equipment such as the solar array itself. Self-deployable, self-stiffening, and retractable structures (SDSRs) do not require the use of external support structures and thus free up volume to be used more efficiently.

4.2 Background

4.2.1 Pehrson's SDSR Work

An aluminum SDSR prototype is shown in Figure 4.1 in the stowed and deployed configurations. The SDSR arrays developed by Pehrson [40] are inspired by origami flasher patterns. Flashers are a subset of general category of miura-ori rings explored by origami artists and engineers such as Robert Lang [personal communication, 2019]. Flashers are inherently useful when a sheetlike structure is deployed from around a central hub and needs to collapse to a compact configuration [41].

SDSRs achieve stiffness throughout deployment by utilizing strain energy of compliant joints (along minor folds) and torsional spring revolute joints (along major folds) (Figure 4.2). The joints are strained as cables threaded through the panels are reeled around a central hub and the array folds around itself as shown in Figure 4.1a. Using compliant joints allows the possibility that

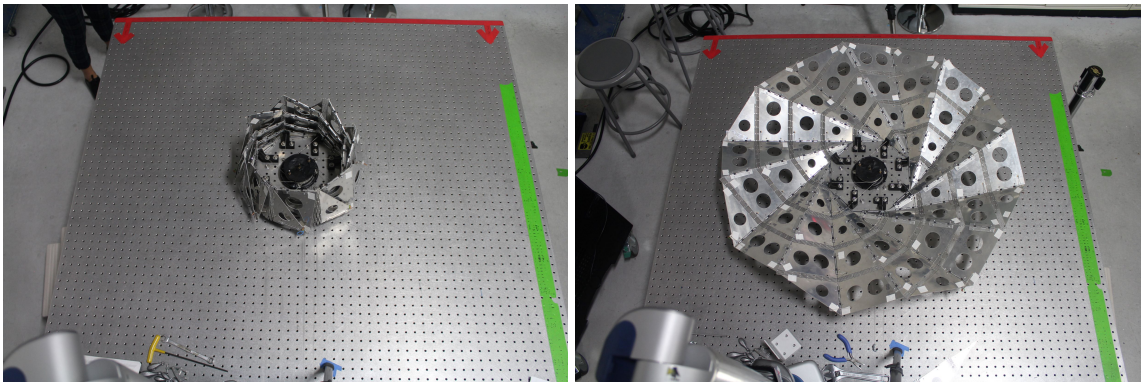

(a) Stowed array (b) Deployed Array

Figure 4.1: Aluminum SDSR array in stowed and deployed positions

the entire array could be cut from one sheet of material, but for large structures, this is impractical. Instead, using compliant joints along the minor folds allows for the array to be divided into monolithic gores that can be cut out of manageably sized sheet materials. The gores can then be assembled into a large array using revolute spring hinges as demonstrated.

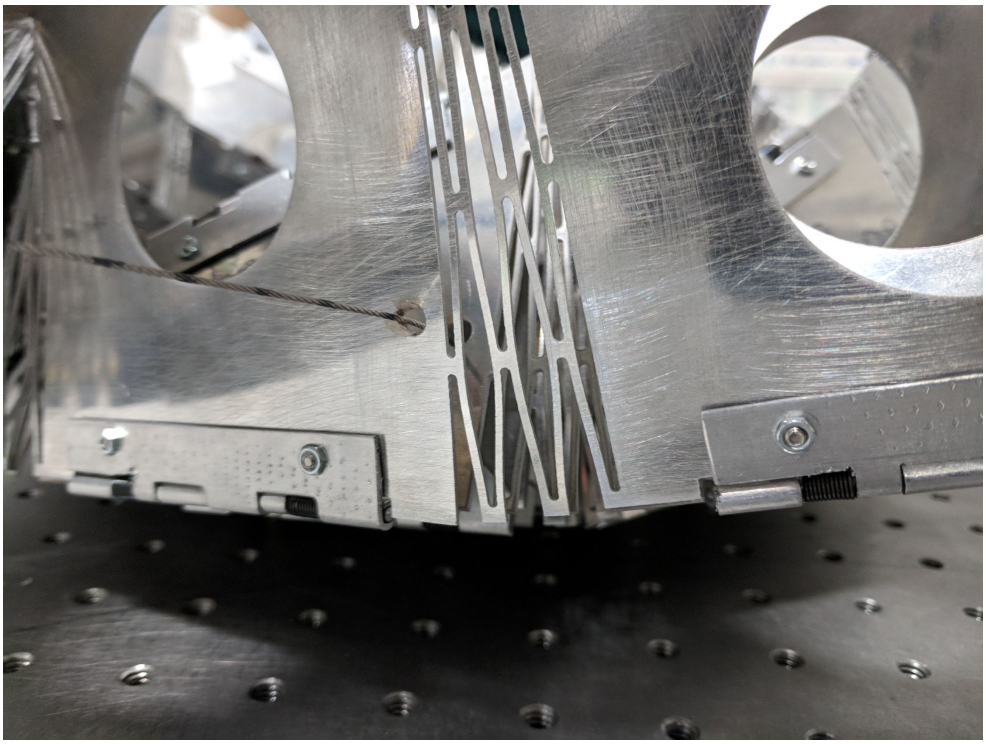

Figure 4.2: Actuation is possible due to strained LET joints and reeling cables

4.2.2 CFRP Compliant Mechanisms

An important consideration in origami engineering is the material. As seen in many origami pieces, the structure of paper makes it an ideal material to produce compliant hinges. When folded, paper fibers delaminate in such a way that reduces the stiffness significantly along the fold creating an axis that the paper can rotate about 360 degrees. Since most engineering materials cannot be folded, origami inspired engineering designs often utilize hinges [24] that can act as a surrogate fold. Traditional hinges are an easy off-the-shelf solution, but are not ideal for low-weight, low-part-count applications. Compliant mechanisms can be excellent surrogate folds for light weight, low part count origami inspired designs [42] because of their ability to attain the large deflections necessary to achieve hinge-like motion.

Fiber reinforced polymer composites are generally used for their high stiffness and low weight properties. Flexible, high-strain composites are becoming more common. For example, thin composite shells are currently finding success as collapsible and coil-able booms in space applications [43, 44]. These high-strain structures show promise for adopting composite materials in other compliant mechanisms such as surrogate folds. Using composites as a fold has it's complications. Making composites thinner to obtain folding motion will not be sufficient in origami inspired designs due to the large bending radii, however, other mechanisms mitigate this problem.

One class of compliant joints proposed for the SDSR are lamina emergent torsional (LET) joints. A LET joint is a network of beams oriented to either bend around their long or short length axis (making them a bending segment or torsion segment). The total stiffness of the joint can be determined by determining the spring constants of each segment and adding them in parallel or series according to their configuration in the joint [29]. LET joint analysis assumes an isotropic material. Because equivalent stiffness calculations in fiber reinforced materials rely not only on the geometry of the joint members, but also on the fiber orientation throughout the laminate (ply layup), LET joints in anisotropic materials such as CFRP's have yet to be addressed in the literature.

Failure mechanisms in composites can be catastrophic and difficult to predict. Composite laminates can be weakened due to voids or inclusions that are difficult to detect. Delamination and fracture are common in high-strain situations. It is hoped to better understand the limits of reliability and fatigue in composite flexure joints used in an SDSR array, however, this work only considers basic elements of structural and material failure. Even so, failure can be considered

Figure 4.3: Unstrained LET joint With $[90,90,0]_s$ ply schedule

Figure 4.4: Strained LET joint with $[90,90,0]_s$ ply schedule

in different ways since material failure is a nuanced topic in composite laminates. Because strain energy stored in the deflected joints is needed for actuation of the overall mechanism, a reduction in stiffness that does not allow for reliable array deployment could be considered failure. High cycle fatigue testing and testing in extreme environmental conditions would be valuable to consider for future work.

4.3 Design

4.3.1 Joint Design

A LET joint was chosen for the minor folds of the SDSR array. Because the gores are triangular in shape, there will be a difference in length of the torsional members across the entire joint. Variation in length leads to a non-constant stiffness, and thus greater stresses in the stiffest (shortest) torsional members and larger deflections in the longest members. It is possible to mitigate this stiffness disparity across the joint by varying the width of the torsional members, however, that will be addressed in future work. The present design employs constant width torsional members where the equivalent stiffness of the joint used is an average stiffness.

One drawback usually associated with LET joints is called parasitic motion, or motion in any direction or about any axis other than the one intended. This becomes an advantage for using it in the flasher pattern chosen for the array because it is not rigidly foldable; i.e. the array could not fold without the parasitic motion [40].

4.3.2 Panel Design

While the novelty of this work is on the joint design, analysis of the panels is critical because they determine the use case of the array. For example, flatness is very important in antenna design and the following analysis would help determine whether this could be an acceptable design solution. In this section, only the largest panel in the array is analysed as the smaller panels will have less deflection. The panel is a non-rectangular quadrilateral (see Figure 4.1b where the joints along each edge apply moments on the panel. On the long edges, the LET joints apply a symmetric moment load. On the short edges, the spring loaded pin-joints apply an anti-symmetric load.

Because most analytical solutions are presented for rectangular panels, the quadrilateral panel was considered as a rectangular panel in order to perform analytical calculations. That solution will be used in future work to validate an FEA solution which could be extended to the quadrilateral panel. Fig. 4.5 shows the rectangular panel with the combined load case separated into two different load cases which will be superimposed to create the total deflection solution.

As the loading cases examined in this class did not examine bending loads, a model allowing for a bending moment had to be constructed from other sources as the basis for this model.

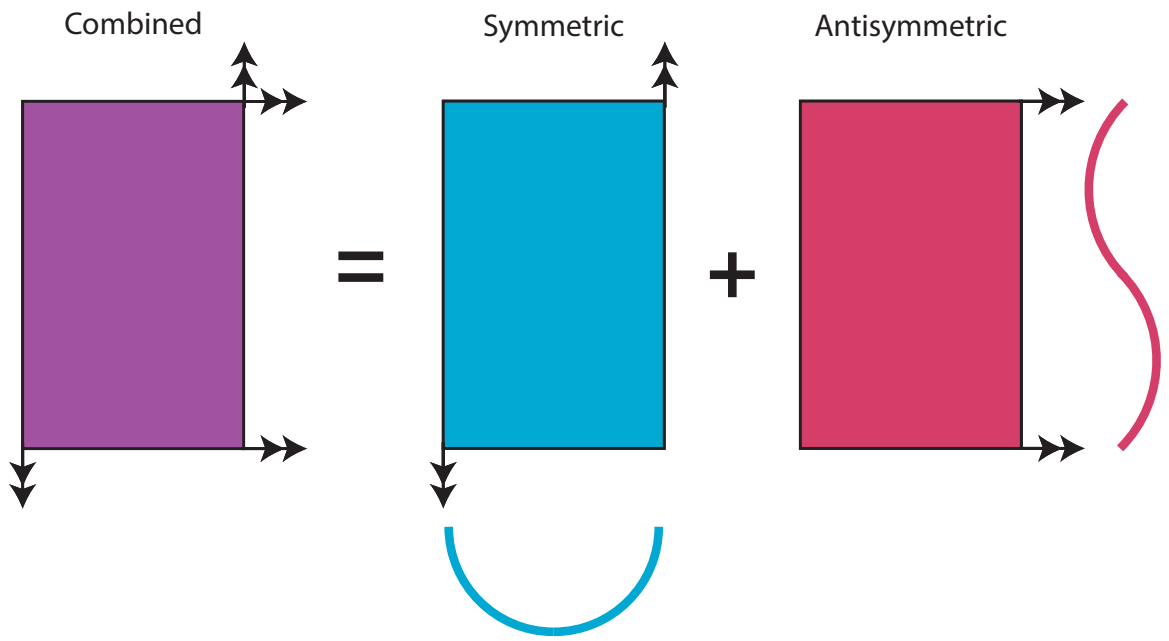

Figure 4.5: The loading case of the rectangular panel split into the symmetric and anti-symmetric load cases to be solved and then superimposed.

Kurata [45] provides the solution for a simply supported, isotropic plate with clamped edge conditions on portions of each edge of the plate. The equations for symmetric and anti-symmetric moment loadings were taken from Kurata and modified to account for the moment loadings occurring uniformly along each edge. Because Kurata's work is for isotropic plates, the overall flexural rigidity (D) of the plate needed to be used. It is given by Timoshenko [46] as

$$D = \frac{Eh^3}{12(1-\nu^2)} \tag{4.1}$$

Because the design is dependent on orthotropic plies forming a laminate, this equation cannot be used in this form because the flexural rigidity is not the same in every direction. In order to account for this change, the flexural rigidity was modified by using smeared stiffness properties of the composite laminate as a whole. From Kassapaglou [47], for a symmetric laminate, the effective bending moduli and Poisson's ratios in the fiber and matrix directions, respectively, is

$$E_{1b} = \frac{12}{h^3 d_{11}}, \nu_{12b} = -\frac{d_{12}}{d_{11}} \tag{4.2}$$

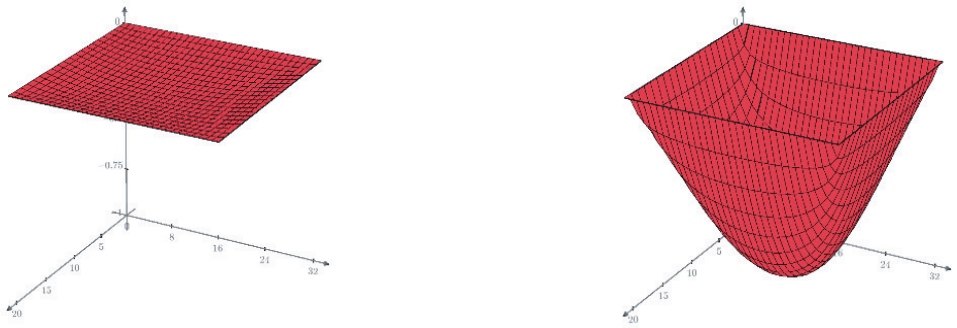

(a) (b)

Figure 4.6: The deflection of the panel due to the symmetric moment loading on the long edges. (a) The actual deflection (b) A view of the deflection with an exaggerated z-axis (minimum value on the z-axis is -0.06 mm).

$$E_{2b} = \frac{12}{h^3 d_{22}}, \nu_{21b} = -\frac{d_{12}}{d_{22}} \tag{4.3}$$

Where d_{11}, d_{12}, d_{22} are the values at the matrix locations of d, and d is the inverse of the D matrix in the ABD matrix, when the laminate is symmetric. Substituting these values into Eqn. 4.1 yields

$$D_1 = \frac{1}{d_{11}(1 - \frac{d_{12}}{d_{11}}^2)} \tag{4.4}$$

$$D_2 = \frac{1}{d_{22}(1 - \frac{d_{12}}{d_{22}}^2)} \tag{4.5}$$

Substituting these into the equations for the deflection due to symmetric loading and anti-symmetric loading yields

$$w_{symmetric} = \frac{8M_y a^2}{\pi^3 D_1 b} \sum_{m=1,3..}^{\infty} \sum_{n=1,3,..}^{\infty} \frac{m}{(m^2 + \frac{a^2}{b^2} n^2)^2} sin(\frac{m\pi x}{a}) sin(\frac{n\pi y}{b}) \tag{4.6}$$

and

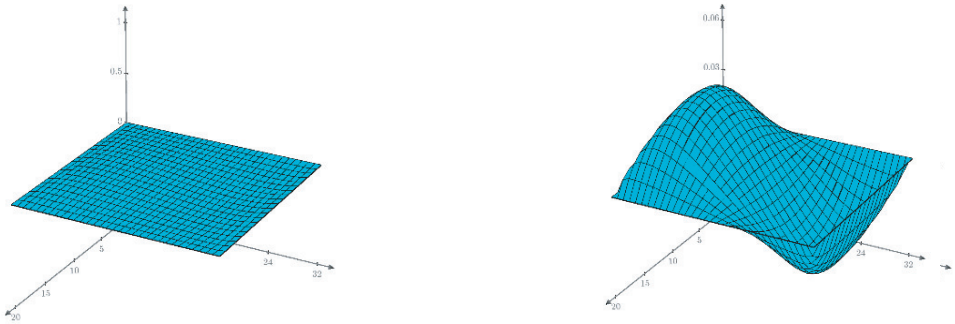

(a) (b)

Figure 4.7: The deflection of the panel due to the antisymmetric moment loading on the short edges. (a) The actual deflection (b) A view of the deflection with an exaggerated z-axis (minimum value on the z-axis is -0.06 mm).

$$w_{asymmetric} = \frac{8M_x a^2}{\pi^3 D_2 b} \sum_{m=2,4..}^{\infty} \sum_{n=1,3,..}^{\infty} \frac{m}{(m^2 + \frac{b^2}{a^2} n^2)^2} sin(\frac{m\pi x}{a}) sin(\frac{n\pi y}{b}) \tag{4.7}$$

where M_y is the moment about the $y-axis$, M_x is the moment about the $x-axis$, a is the length of the panel, and b is the width of the panel. The combined deflection is the sum of these two terms, or

$$\begin{aligned} w_{combined} = & \frac{8M_y a^2}{\pi^3 D_1 b} \sum_{m=1,3..}^{\infty} \sum_{n=1,3,..}^{\infty} \frac{m}{(m^2 + \frac{a^2}{b^2} n^2)^2} sin(\frac{m\pi x}{a}) sin(\frac{n\pi y}{b}) \\ & + \frac{8M_x a^2}{\pi^3 D_2 b} \sum_{m=2,4..}^{\infty} \sum_{n=1,3,..}^{\infty} \frac{m}{(m^2 + \frac{b^2}{a^2} n^2)^2} sin(\frac{m\pi x}{a}) sin(\frac{n\pi y}{b}) \end{aligned} \tag{4.8}$$

The deflections for each case, shown separately in Fig. 4.6 and Fig. 4.7, respectively, were then summed to find the total deflection due to both loading conditions. The combined deflection is

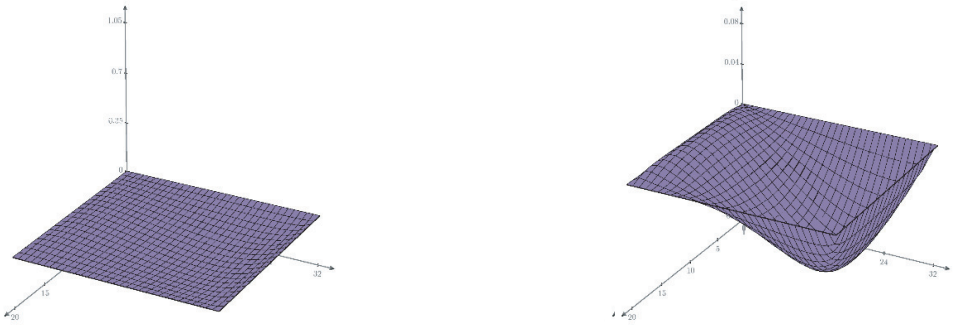

(a) (b)

Figure 4.8: The deflection of the panel due to the combined moment loading on the edges. (a) The actual deflection (b) A view of the deflection with an exaggerated z-axis (minimum value on the z-axis is -0.12 mm).

shown in Fig. 4.8. For all three figures, subfigure (b) is an exaggerated view to make the deflections more visible.

4.4 Hardware Demonstration

Two small CFRP SDSR prototypes were constructed to demonstrate proof of concept. In both prototypes, rivets were used to mount the major fold hinges to the panels because of their simplicity, although it is recognized that rivets are generally not used for fastening composite panels due to possible delamination effects.

The gores were cut from CFRP panels fabricated with prepreg designed for use in autoclave tooling applications. The panels are three plies thick and were cured out-of-autoclave under vacuum.

4.4.1 First Prototype

Figure 4.9 shows the initial CFRP SDSR prototype which had two important successes. It demonstrated proof of concept and exposed flaws in the design for further correction. On the first retraction, the small bending segments in the most central LET joints experienced some material failure. Some bending members failed completely after successive cycles (see Figure 4.11). One initial oversight was the interference created by the thickness of the hinges near the central hub

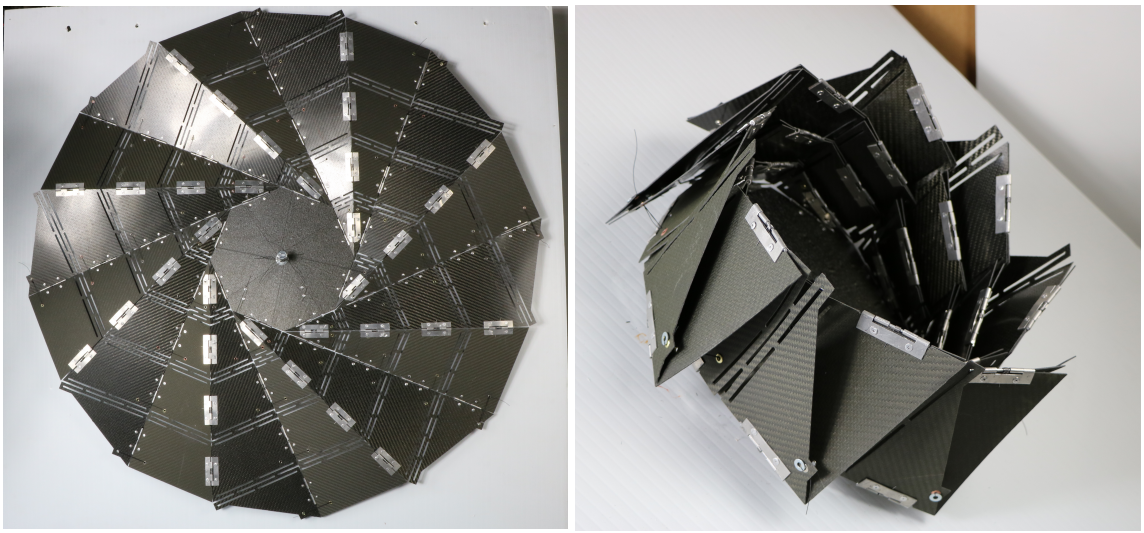

(a) Composite SDSR prototype deployed (b) Composite SDSR prototype stowed

Figure 4.9: Initial carbon composite SDSR array in deployed and stowed positions

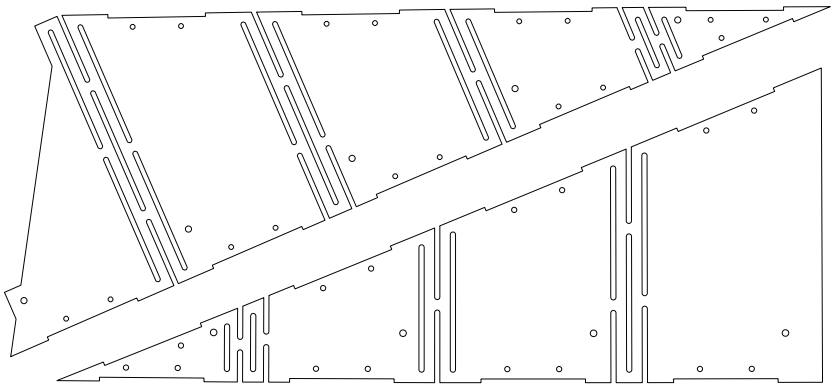

Figure 4.10: Drawing of first iteration gores with innermost LET joints that failed

which caused greater stress than anticipated in the more centrally located joints. Even with the failed joints, the mechanism functioned because it is a significantly over-constrained system.

4.4.2 Second Prototype

Two problems were addressed in the second iteration prototype. First, the failure of the bending segments of the first prototype was due to the parasitic motion of the joint. The bending member is too stiff in torsion and the stress increases dramatically. Because the SDSR is not flat-foldable, this parasitic motion is necessary for actuation, but the bending members could not

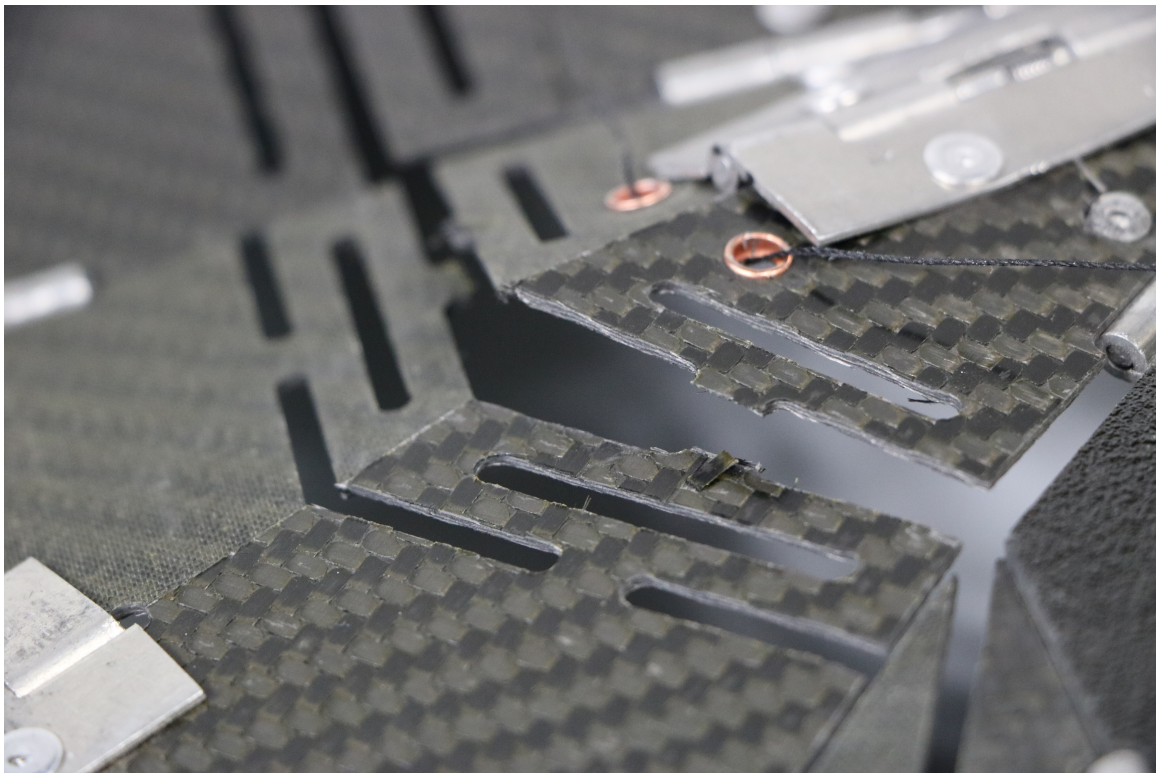

Figure 4.11: Anticipated LET joint failure in

sustain the stresses. The torsional members are also stiff in bending which transfers stress more easily to the bending members in torsion. To avoid this failure, the inner-most LET joints were redesigned to eliminate the bending segments entirely as shown in Figure 4.13. The second issue resolved were the aluminum hinges. They were too thick and caused interference in the folding of the mechanism, especially in the innermost joints. The revolute joints were replaced with aramid fabric and carbon fiber plates (See Figure 4.12).

4.5 Future Work

Better models for anisotropic LET arrays will need to be developed for future design iterations. The panel analysis can be sufficient depending on the deployable array's use case. LET joint properties need further characterization to ensure a predictable design. To assess the reliability and robustness of the system, dynamic and modal analysis will need to be developed. Controlled hardware tests (as well as fatigue and extreme environmental testing) would need to be compared to the analytical model solutions as well as FEA to gain further confidence in the models.

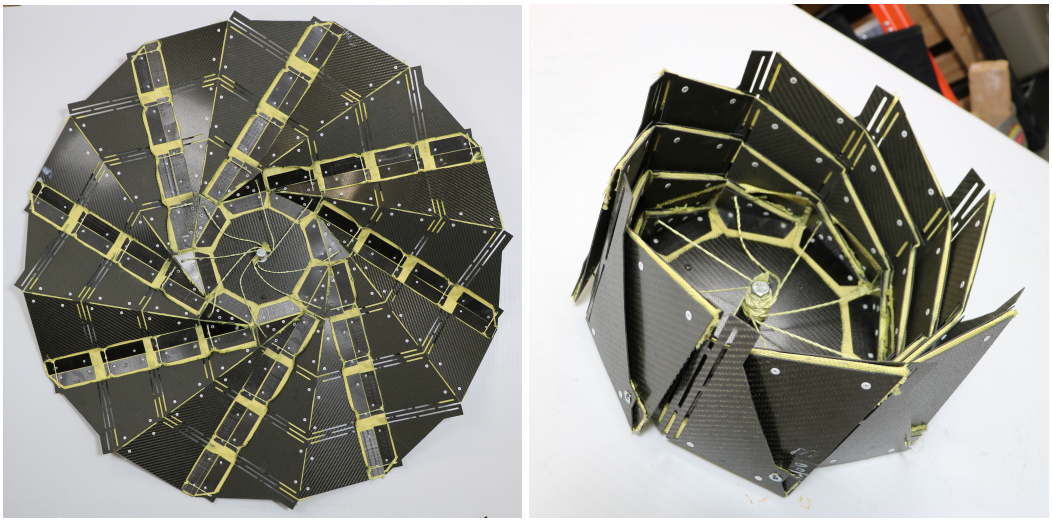

(a) Composite SDSR prototype deployed (b) Composite SDSR prototype stowed

Figure 4.12: Second iteration carbon composite SDSR array with aramid fabric hinges in deployed and stowed positions

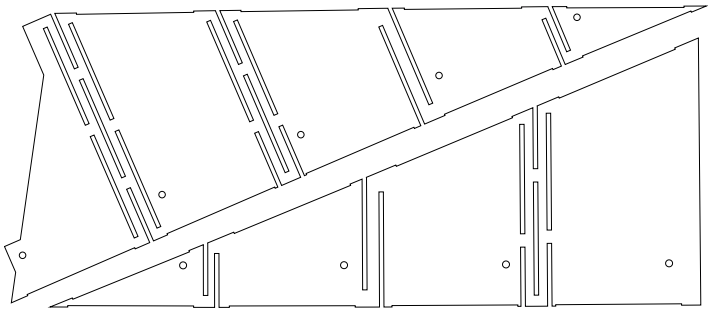

Figure 4.13: Drawing of second iteration gores with innermost LET joints redesigned

4.6 Conclusion

SDSRs are innovative and versatile structures that can enhance the effectiveness of spacecraft to fulfil their missions. They use limited space more efficiently, have a simple deployment system, they can be retracted and also tuned to many configurations. The successful prototype and analysis presented on advanced composite construction of SDSR's incorporating flexural hinges validates the need for further research and development.

CHAPTER 5. CONCLUSION

The objective of this thesis is to develop and demonstrate techniques for designing origami-based mechanical systems utilizing compliant composite joints with special application to deployable space structures. The objective is met by exploring the adaptation of LET arrays into origami inspired mechanisms, incorporating principles of high-strain composites into LET arrays, and then demonstrating the utility of composite LET arrays in a unique deployable mechanical system. Results from analysis, modeling, prototyping, and empirical testing indicate that (while not as compact as their isotropic material counterparts) composite LET joints can be used as surrogate folds in SDSR arrays. Furthermore, the techniques presented in this thesis create the possibility of expanding the feasibility of using origami-based design by expanding the design space of origami mechanisms that move and deploy.

By developing design concepts and models for atypical materials and geometric configurations of LET arrays, this work contributes to the knowledge base of high-strain composites, compliant mechanisms, and origami-based mechanical systems. Through this research, engineers, designers, and academics are better equipped to use composite LET joints in structure and mechanism design.

This work could be continued by developed more in-depth models and analytical tools for developing composite LET joints and integrating them into applications. Manufacturing processes could be develop to integrate composite LETs more easily into structures and laminates.

REFERENCES

[1] Jacobsen, J., Winder, B., Howell, L., and Magleby, S., 2010. "Lamina emergent mechanisms and their basic elements." *Journal of Mechanisms and Robotics,* **2**(1), pp. 1–9. 4

[2] Lusk, C. P., and Howell, L. L., 2008. "Components, building blocks, and demonstrations of spherical mechanisms in microelectromechanical systems." *Journal of Mechanical Design, Transactions of the ASME,* **130**(3), mar. 4

[3] Greenberg, H., 2012. "The Application of Origami to the Design of Lamina Emergent Mechanisms (LEMs) with Extensions to Collapsible, Compliant, and Flat Folding Mechanisms." MS Thesis, Brigham Young University, Provo, UT. 4

[4] Pehrson, N. A., Magleby, S. P., Lang, R. J., and Howell, L. L., 2016. "Introduction of monolithic origami with thick-sheet materials." In *International Association for Shell and Spatial Structures*, International Association of Shells and Spatial Structures. 4

[5] Chen, G., Magleby, S. P., and Howell, L. L., 2018. "Membrane-Enhanced Lamina Emergent Torsional Joints for Surrogate Folds." *Journal of Mechanical Design, Transactions of the ASME,* **140**(6), jun. 5

[6] Andrews, D. W., Magleby, S. P., and Howell, L. L., 2020. "Thickness-utilizing deployable hard stops for origami-based design applications." *Mechanical Sciences,* **11**(2), oct, pp. 395–410. 5

[7] Chen, G., and Howell, L. L., 2009. "Two general solutions of torsional compliance for variable rectangular cross-section hinges in compliant mechanisms." *Precision Engineering,* **33**(3), pp. 268–274. 5

[8] Pehrson, N. A., Bilancia, P., Magleby, S., and Howell, L., 2020. "Load-displacement characterization in three degrees-of-freedom for general lamina emergent torsion arrays." *Journal of Mechanical Design, Transactions of the ASME,* **142**(9), sep. 5

[9] Nelson, T. G., Baldelomar Pinto, L., Bruton, J. T., Deng, Z., Nelson, C. G., and Howell, L. L., 2021. "Deployable Convex Generalized Cylindrical Surfaces Using Torsional Joints." *Journal of Mechanisms and Robotics*, jan, pp. 1–13. 6

[10] Young, W. C., and Budynas, R. G., 1976. Roark's Formulas for Stress and Strain Tech. rep. 9

[11] Chen, G., and Howell, L. L., 2017. "Symmetric equations for evaluating maximum torsion stress of rectangular beams in compliant mechanisms." *submitted to Chinese Journal of Mechanical Engineering*. 9

[12] Strong, A. B., 2005. *Plastics: Materials and Processing, 3rd Edition*. Pearson. 13

[13] Howell, L. L., Magleby, S. P., and Olsen, B. M., 2013. *Handbook of compliant mechanisms*. John Wiley & Sons. 15

[14] Merriam, E. G., Jones, J. E., and Howell, L. L. Design of 3D-Printed Titanium Compliant Mechanisms Tech. rep. 15

[15] Bigelow Aerospace. 15

[16] Leclerc, C., and Pellegrino, S. Reducing Stress Concentration in the Transition Region of Coilable Ultra-Thin-Shell Booms Tech. rep. 15

[17] Mallikarachchi, H. M., and Pellegrino, S., 2014. "Design of Ultrathin composite self-deployable booms." *Journal of Spacecraft and Rockets,* **51**(6), nov, pp. 1811–1821. 15

[18] Banik, J., Kiefer, S., Lapointe, M., and Lacorte, P., 2018. "On-orbit validation of the roll-out solar array." In *IEEE Aerospace Conference Proceedings*, Vol. 2018-March, IEEE Computer Society, pp. 1–9. 15

[19] Silver, M. J., Echtery, M. A., Reidz, B. M., and Banikx, J. A., 2016. "Precision high-strain composite hinges for the deployable in-space coherent imaging telescope." In *3rd AIAA Spacecraft Structures Conference*, American Institute of Aeronautics and Astronautics Inc, AIAA. 15

[20] Delimont, I. L., 2014. "Compliant joints suitable for use as surrogate folds." Master's thesis, Brigham Young University. 16

[21] Chen, Y., Peng, R., and You, Z., 2015. "Origami of thick panels." *Science,* **349**(6246), pp. 396–400. 16

[22] Butler, J., Pehrson, N., and Magleby, S., 2019. "Thick folding through regionally-sandwiched compliant sheets." In *Proceedings of the ASME Design Engineering Technical Conference*, Vol. 5B-2019, American Society of Mechanical Engineers (ASME). 16

[23] Tachi, T., 2016. "Rigid-foldable thick origami." In *Origami 5: Fifth International Meeting of Origami Science, Mathematics, and Education*. CRC Press, apr, pp. 253–263. 16

[24] Lang, R. J., Tolman, K. A., Crampton, E. B., Magleby, S. P., and Howell, L. L., 2017. "A review of thickness-accommodation techniques in origami-inspired engineering." *Applied Mechanics Reviews* Article in press. 16, 32

[25] Edmondson, B. J., Lang, R. J., Magleby, S. P., and Howell, L. L., 2014. "An Offset Panel Technique for Thick Rigidily Foldable Origami." ASME International. 16

[26] Nelson, T. G., Lang, R. J., Magleby, S. P., and Howell, L. L., 2018. "Implementation of Rolling Contacts for SORCE Joints." In *2018 International Conference on Reconfigurable Mechanisms and Robots, ReMAR 2018 - Proceedings*, Institute of Electrical and Electronics Engineers Inc. 16

[27] Zirbel, S. A., Wilson, M. E., Magleby, S. P., and Howell, L. L., 2013. "An origami-inspired self-deployable array." In *Proceedings of the ASME 2013 Conference on Smart Materials, Adaptive Structures and Intelligent Systems*. 16

[28] Lang, R. J., Brown, N., Ignaut, B., Magleby, S., and Howell, L., 2020. "Rigidly Foldable Thick Origami Using Designed-Offset Linkages." *Journal of Mechanisms and Robotics,* **12**(2), apr. 16

[29] Jacobsen, J. O., Chen, G., Howell, L. L., and Magleby, S. P., 2009. "Lamina emergent torsional (LET) joint." *Mechanism and Machine Theory,* **44**, pp. 2098 – 2109. 17, 32

[30] Barbero, E. J., 2017. *Introduction to Composite Materials Design, Third Edition*. CRC Press, oct. 18

[31] Lekhnitskii, S. G., 1963. *Theory of Elasticity of an Anisotropic Elastic Body*. San Francisco, USA: Holden-Day. 18

[32] Powell, J., Maise, G., and Paniagua, J., 2001. "MIC - A self deploying magnetically inflated cable system for large scale space structures." *Acta Astronautica,* **48**(5-12), jun, pp. 331–352. 30

[33] Qi, X., Huang, H., Li, B., and Deng, Z., 2016. "A large ring deployable mechanism for space satellite antenna." *Aerospace Science and Technology,* **58**, pp. 498 – 510. 30

[34] McEachen, M. E., 2018. "Compact Telescoping Array: Advancement from Concept to Reality." In *2018 AIAA Spacecraft Structures Conference*, American Institute of Aeronautics and Astronautics. 30

[35] Mikulas, M. M., Pappa, R. S., Warren, J., and Rose, G., 2015. "Telescoping solar array concept for achieving high packaging efficiency." AIAA SciTech Forum. American Institute of Aeronautics and Astronautics, Jan. 30

[36] Francis, W. H., Davis, B., and Lake, M., 2016. "Robust, highly scalable solar array system." AIAA SciTech Forum. American Institute of Aeronautics and Astronautics, Jan. 30

[37] Guo, H., Liu, R., Deng, Z., and Zhang, J., 2011. "Dynamic characteristic analysis of large space deployable articulated mast." *Procedia Engineering,* **16**, pp. 716 – 722 International Workshop on Automobile, Power and Energy Engineering. 30

[38] Wilson, L. L., 2017. "Analysis of packaging and deployment of ultralight space structures." PhD thesis. 30

[39] Schenk, M., Viquerat, A. D., Seffen, K. A., and Guest, S. D., 2014. "Review of inflatable booms for deployable space structures: packing and rigidization." *Journal of Spacecraft and Rockets*. 30

[40] Pehrson, N. A., Smith, S. P., Ames, D. C., Magleby, S. P., and Arya, M., 2019. "Self-Deployable, Self-Stiffening, and Retractable Origami-Based Arrays for Spacecraft." In *AIAA Scitech 2019 Forum*, American Institute of Aeronautics and Astronautics. 30, 34

[41] Zirbel, S. A., Wilson, M. E., Magleby, S. P., and Howell, L. L., 2013. "An Origami-Inspired Self-Deployable Array." In *Volume 1: Development and Characterization of Multifunctional Materials; Modeling, Simulation and Control of Adaptive Systems; Integrated System Design and Implementation*. 30

[42] Delimont, I. L., Magleby, S. P., and Howell, L. L., 2015. "A family of dual-segment compliant joints suitable for use as surrogate folds." *Journal of Mechanical Design,* **137**(9). 32

[43] Ferraro, S., and Pellegrino, S., 2018. "Self-Deployable Joints for Ultra-Light Space Structures." In *2018 AIAA Spacecraft Structures Conference*, American Institute of Aeronautics and Astronautics. 32

[44] Fernandez, J. M., Rose, G., Stohlman, O. R., Younger, C. J., Dean, G. D., Warren, J. E., Kang, J. H., Bryant, R. G., and Wilkie, K. W., 2018. "An Advanced Composites-Based Solar Sail System for Interplanetary Small Satellite Missions." In *2018 AIAA Spacecraft Structures Conference*, American Institute of Aeronautics and Astronautics. 32

[45] Kurata, M., 1960. "Bending of simply supported rectangular plates with clamped portions along arbitrary sections of the edges." *Ingenieur-Archiv,* **27**(6), pp. 385–416. 35

[46] Timoshenko, S. P., and Woinowsky-Krieger, S., 1959. *Theory of plates and shells*. McGraw-hill. 35

[47] Kassapoglou, C., 2013. *Design and analysis of composite structures: with applications to aerospace structures*. John Wiley & Sons. 35

APPENDIX A. ANSYS MECHANICAL APDL SCRIPT

A.1 Inside LET Joint

```
fini
/cle

eps=1e-6
mm=1e-3
MPa=1e6
pg=acos(-1)
RTOD=180/pg

!Material properties
E1x=15000*MPa
E1y=15000*MPa
E1z=5000*MPa
pr1x=0.3
pr1y=0.3
pr1z=0.3
G1xy=1300*MPa
G1xz=1300*MPa
G1yz=1900*MPa

!Geometry (4 Layers)
t1=0.5*mm
t2=0.5*mm
t3=0.5*mm
t4=0.5*mm

Lc=3.175*mm
Lb=3.175*mm
w=50.8*mm
wc=6.35*mm
wb=6.35*mm
wt=1*3.175*mm/2 !change
t=2*mm

!Deflection Angle
theta=35

!Geometrical relations
L=2*(Lb+wt)+Lc
Lext=0.5*L
Ls=Lext+Lb+wt
deltax_load=w/2

!Element size (ratio of length L)
siz=L/25 !30 for Outside LET

!# of FEA substeps
substeps=10

/prep7

!Material properties assignment
mp,ex,1,E1x
mp,ey,1,E1y
mp,ez,1,E1z
mp,prxy,1,pr1x
mp,pryz,1,pr1y
mp,prxz,1,pr1z
mp,Gxy,1,G1xy
mp,Gyz,1,G1yz
mp,Gxz,1,G1xz

!Geometry Definition
k,1,-Ls-Lc/2,0,0
k,2,-Ls-Lc/2,0,-w
k,3,-Lc/2,0,0
k,4,-Lc/2,0,-w
k,5,-Lc/2,0,-w/2+wc/2
k,6,-Lc/2,0,-w/2-wc/2
k,7,0,0,-w/2+wc/2
k,8,0,0,-w/2-wc/2
k,9,-Ls-Lc/2+Lext,0,-wb
k,10,-Ls-Lc/2+Lext,0,-w+wb
k,11,-Lc/2-wt,0,-wb
k,12,-Lc/2-wt,0,-w+wb

a,1,2,4,6,8,7,5,3,1
a,9,10,12,11

asba,1,2
numc,area
csys,0

et,1,181
keyopt,1,3,2    !full integration
keyopt,1,8,1

sectype,1,shell

!secdata,thick,mat#,Angle,IntPoints
secdata,t1,1,0,3
```

```
secdata,t2,1,45,3
secdata,t3,1,45,3
secdata,t4,1,0,3

mshk,2

lesi,1,,,w/siz
lesi,3,,,(w-wc)/(2*siz)
lesi,7,,,(w-wc)/(2*siz)
lesi,5,,,wc/siz

esiz,siz
amesh,all

/nerr,0
numm,node,1e-6 !Merge node command
arsy,x,all !Symmetric command
numm,node,1e-6

et,2,184
keyopt,2,1,1
keyopt,2,2,1
type,2

!defining Load Node
*get,Numax,node,,num,max
n,Numax+1,Lc/2+Ls+deltax_load,0,-w/2
csys,0

lsel,s,line,,13 !Select line
nsll,s,1 !Select all the nodes
*vget,Nodesel,node1,,nlist !Make vect
*get,num,node,,count
alls

*do,i,1,num
e,Numax+1,Nodesel(i) !Create elements
*enddo
eplot

lsel,s,line,,1
nsll,s,1
d,all,all !Select line, fix all
alls

d,Numax+1,rotz,theta/RTOD
!Change axis for Twisting
!d,Numax+1,rotx,theta/RTOD

/nerr,defa

fini
/solu

!***Section 5: Solver Parameters***
antype, static
nlgeom,on
autots,off
nsubst,substeps
outre,all,all
solve

fini
/post1

!***Section 6: Post Processing***
set,last

*get,rot,node,Numax+1,rot,z  !rotz
*get,Mom,node,Numax+1,rf,mz  !react momt
!Change Axis for Twisting
!*get,rot,node,Numax+1,rot,x  !rotx
!*get,Mom,node,Numax+1,rf,mx  !react momt

esel,s,type,,1
etable,sig,s,eqv
esort,etab,sig
*get,sigma,sort,,max
alls

Moment=Mom/mm
Angle = rot*RTOD
Stress=sigma/MPa
Stiffness = Moment/rot
```

A.2 Outside LET Joint

```
fini
/cle

eps=1e-6
mm=1e-3
MPa=1e6
pg=acos(-1)
RTOD=180/pg

!Material properties

!Layers
E1x=15000*MPa
E1y=15000*MPa
E1z=5000*MPa
pr1x=0.3
pr1y=0.3
pr1z=0.3
G1xy=1300*MPa
G1xz=1300*MPa
```

```
G1yz=1900*MPa

!Geometry (4 Layers)

t1=0.5*mm
t2=0.5*mm
t3=0.5*mm
t4=0.5*mm

Lc=3.175*mm
Lb=3.175*mm
w=50.8*mm
wc=6.35*mm
wb=6.35*mm
wt=6*3.175*mm/2 !change
t=2*mm

!Deflection Angle
theta=35

!Geometrical relations
L=2*(Lb+wt)+Lc
Lext=0.5*L
Ls=Lext+Lb+wt
deltax_load=w/2

!Element size (ratio of length L)
siz=L/30
!Number of FEA substeps
substeps=10

/prep7

!Material properties assignment
mp,ex,1,E1x
mp,ey,1,E1y
mp,ez,1,E1z
mp,prxy,1,pr1x
mp,pryz,1,pr1y
mp,prxz,1,pr1z
mp,Gxy,1,G1xy
mp,Gyz,1,G1yz
mp,Gxz,1,G1xz

!Geometry Definition
k,1,-Ls-Lc/2,0,0
k,2,-Ls-Lc/2,0,-w
k,3,-Lc/2-wt-Lc,0,0
k,4,-Lc/2-wt-Lc,0,-w/2+wb/2
k,5,-Lc/2-wt,0,-w/2+wb/2
k,6,-Lc/2-wt,0,0
k,7,0,0,0
k,8,0,0,-wc
k,9,-Lc/2,0,-wc
k,10,-Lc/2,0,-w+wc
k,11,0,0,-w+wc
k,12,0,0,-w
k,13,-Lc/2-wt,0,-w
k,14,-Lc/2-wt,0,-w/2-wb/2
k,15,-Lc/2-wt-Lc,0,-w/2-wb/2
k,16,-Lc/2-wt-Lc,0,-w

a,1,3,4,5,6,7,8,9,10,
11,12,13,14,15,16,2,1
csys,0

et,1,181
keyopt,1,3,2    ! full integration
keyopt,1,8,1

sectype,1,shell

!secdata,thick,mat#,Angle,IntPoints
secdata,t1,1,0,3
secdata,t2,1,45,3
secdata,t3,1,45,3
secdata,t4,1,0,3

mshk,2

lesi,16,,,w/siz
lesi,2,,,(w-wc)/(2*siz)
lesi,4,,,(w-wc)/(2*siz)
lesi,6,,,wc/siz
lesi,8,,,(w-(2*wc))/siz
lesi,10,,,wc/siz
lesi,12,,,(w-wc)/(2*siz)
lesi,14,,,(w-wc)/(2*siz)

esiz,siz
amesh,all

/nerr,0
numm,node,1e-6 !Merge node command
arsy,x,all !Symmetric command
numm,node,1e-6

et,2,184
keyopt,2,1,1
keyopt,2,2,1
type,2

!define Load Node
*get,Numax,node,,num,max
n,Numax+1,Lc/2+Ls+deltax_load,0,-w/2
csys,0
lsel,s,line,,32 !Select line
nsll,s,1 !Select all nodes on line
*vget,Nodesel,node1,,nlist !Make vect
*get,num,node,,count
alls

*do,i,1,num
e,Numax+1,Nodesel(i) !Create elements
*enddo
eplot

lsel,s,line,,16
```

```
nsll,s,16
d,all,all !Select line 16, fix all
alls

d,Numax+1,rotz,theta/RTOD
!Change axis for Twisting
!d,Numax+1,rotx,theta/RTOD


/nerr,defa

fini
/solu

!***Section 5: Solver Parameters***

antype, static
nlgeom,on
autots,off
nsubst,substeps
outre,all,all
solve

fini
```

```
/post1

!***Section 6: Post Processing***

set,last

*get,rot,node,Numax+1,rot,z  !rotz
*get,Mom,node,Numax+1,rf,mz  !react momt

!Change Axis for Twisting
!*get,rot,node,Numax+1,rot,x  !rotx
!*get,Mom,node,Numax+1,rf,mx  !react momt

esel,s,type,,1
etable,sig,s,eqv
esort,etab,sig
*get,sigma,sort,,max
alls

Moment=Mom/mm
Angle = rot*RTOD
Stress=sigma/MPa
Stiffness = Moment/rot
```

APPENDIX B. MATLAB SCRIPT FOR CFRP LET JOINT DATA

B.1 LET Joint Folding

```
clear all

% Import data from text file

k=0;

for j = 1:6
for i = 1:3

    k=k+1;
    Filename(k) = strcat(num2str(j),strcat("_16_Outside_Sample",num2str(i)));
end
for i = 1:3

    k=k+1;
    Filename(k) = strcat(num2str(j),strcat("_16_Inside_Sample",num2str(i)));
end
end

% Setup the Import Options
opts = delimitedTextImportOptions("NumVariables", 3);

% Specify range and delimiter
opts.DataLines = [25, Inf];
opts.Delimiter = "\t";

% Specify column names and types
opts.VariableNames = ["Var1", "Angle", "Torque"];
opts.SelectedVariableNames = ["Angle", "Torque"];
opts.VariableTypes = ["string", "double", "double"];
opts = setvaropts(opts, 1, "WhitespaceRule", "preserve");
opts = setvaropts(opts, 1, "EmptyFieldRule", "auto");
opts.ExtraColumnsRule = "ignore";
opts.EmptyLineRule = "read";

for i = 1:k

% Import the data
tbl = readtable(strcat("C:\Users\CFRP LET Joints\Data\Bend\",...
    Filename(i)), opts);

% Convert to output type
data{i} = [tbl.Angle, tbl.Torque];

end
```

```
% Clear temporary variables
clear opts tbl

%% Model Stiffness

index = 1
for i = 1:2:12
a = (index/16)*.0254;
b = .002;
L = .0254*.75;
Gxy = 1.3e9;
Gyz = 1.5e9;

n = 1:3:51;
Summation = sum((1./n.^4).*(1-(2.*a./(n.*pi.*b)).*sqrt(Gyz/Gxy).*...
    tanh((n*pi.*b./(2.*a)).*sqrt(Gxy/Gyz))));
Beta = (32*a^2*Gyz)/(pi^4*b^2*Gxy)*Summation;
Kmodel = Gxy*a*b^3*Beta/L

DegModel = 35;
RadModel = DegModel*pi/180;
Tmodel(i) = Kmodel*RadModel*1000
Tmodel(i+1) = Kmodel*RadModel*1000

index = index+1;
end

%% FEA Data

FEAAngles = [5 15 25 35];

FEADataIn =[12.7 38.0 63.4 88.7;
        41.7 125.0 208.4 291.8;
        67.9 203.9 339.9 476.2;
        88.5 265.6 442.9 620.6;
        103.2 309.7 516.5 724.0;
        114.0 342.3 570.9 800.1];

FEADataOut=[12.4 37.1 61.8 86.5;
            40.2 120.7 201.2 281.7;
            62.6 187.8 313.0 438.4;
            79.5 238.5 397.8 557.3;
            89.5 268.6 447.9 627.7;
            99.7 299.3 499.1 699.4];


%% plot all the data

j = 1;
m = 1;

angleload=0;
torqueload=0;
angleunload=0;
torqueunload=0;

for i = 1:3:k
```

```
myfig = figure()

angle1 = data{1,i}(:,1);
torque1 = -data{1,i}(:,2);

angle2 = data{1,i+1}(:,1);
torque2 = -data{1,i+1}(:,2);

angle3 = data{1,i+2}(:,1);
torque3 = -data{1,i+2}(:,2);

% Reduce Data Sets for Plot

% Break into load and unloading sets
p=1;
q=1;
for i = 3:size(angle1)
    if angle1(i)>=angle1(i-2)
        angleload(p)=angle1(i-2);
        torqueload(p)=torque1(i-2);
        p=p+1;
    else
        if angle1(i-2)<28
            angleunload(q)=angle1(i-2);
            torqueunload(q)=torque1(i-2);
            q=q+1;
        end
    end
end

for i = 3:size(angle2)
    if angle2(i)>=angle2(i-2)
        angleload(p)=angle2(i-2);
        torqueload(p)=torque2(i-2);
        p=p+1;
    else
        if angle2(i-2)<28
            angleunload(q)=angle2(i-2);
            torqueunload(q)=torque2(i-2);
            q=q+1;
        end
    end
end

for i = 3:size(angle3)
    if angle3(i)>=angle3(i-2)
        angleload(p)=angle3(i-2);
        torqueload(p)=torque3(i-2);
        p=p+1;
    else
        if angle3(i-2)<28
            angleunload(q)=angle3(i-2);
            torqueunload(q)=torque3(i-2);
            q=q+1;
        end
    end
end

%Add best fit line
```

```
[Loadcoeffs, Sload] = polyfit(angleload,torqueload,1);
LoadFitx = linspace(min(angleload), max(angleload));
[LoadFity,deltaload] = polyval(Loadcoeffs, LoadFitx, Sload);
errxload = [0 5 10 15 20 25 30];
errload = mean(deltaload)*ones(size(errxload))/2;
erryload = polyval(Loadcoeffs, errxload);

[Unloadcoeffs,Sunload] = polyfit(angleunload,torqueunload,1);
UnloadFitx = linspace(min(angleunload), max(angleunload));
[UnloadFity,deltaunload] = polyval(Unloadcoeffs , UnloadFitx, Sunload);
errxunload = [0 5 10 15 20 25];
errunload = mean(deltaunload)*ones(size(errxunload))/3;
erryunload = polyval(Unloadcoeffs, errxunload);

errorbar(errxload, erryload, errload, 'LineWidth',1.5)
hold on
errorbar(errxunload, erryunload, errunload, 'LineWidth',1.5)
plot([0 DegModel],[0 Tmodel(j)],"--k",'LineWidth',1.5)

if round(j/2) == j/2
    titleType = " Inside LET";
    type = "InsideLET";
    plot([0 FEAAngles],[0 FEADataIn(round(j/2),:)],"-kx", ...
        'MarkerSize', 10, 'LineWidth', 1.2)
else
    titleType = " Outside LET";
    type = "OutsideLET";
    plot([0 FEAAngles],[0 FEADataOut(round(j/2),:)],"-kx",...
        'MarkerSize', 10, 'LineWidth', 1.2)
end
legend('Loading','Unloading', 'Lekhnitski', 'FEA', 'Location', 'NorthWest')

title(strcat(strcat(num2str(round(j/2)),"/16"""),titleType))
xlabel('Angle (deg)')
ylabel('Torque (N mm)')
axis([0 35 0 850])
% legend("Sample 1", "Sample 2", "Sample 3", "Location", "northwest")

saveas(myfig,strcat(strcat(strcat(num2str(round(j/2)),"_16"),type),".jpg"))

j = j+1;

end
```